Assistant Prof. Dipl.-Ing. Dr.techn. Andreas Limbeck

TECHNISCHE UNIVERSITÄT WIEN
Vienna University of Technology

Diplomarbeit

"Development of a LA-ICP-MS method for quantitative analysis of Mo, Si and B in oxidation resistant coatings"

ausgeführt am Institut für Chemische Technologien und Analytik

der Technischen Universität Wien

unter der Anleitung von

Assistant Prof. Dipl.-Ing. Dr.techn. Andreas Limbeck

durch Anja Cakara, BSc

Süssenbrunnerstraße 64/4/5,

1220 Wien

Wien, am 30.09.2014

Anja Cakara, BSc

“I thought:

But isn’t this a dance? Isn’t all of this a dance? Isn’t that what we do with words? Isn’t that what we do when we talk, […] when we make plans or leave it to chance? Some of it’s choreographed. Some of the steps have been done for ages. And the rest - the rest is spontaneous. The rest has to be decided on the floor, in the moment, before the music ends.“

Dash and Lily’s Book of Dares, David Levithan

Abstract

Physical vapour deposition (PVD), which is a thin film deposition process, can be divided in various techniques, an important one over the last decades being magnetron sputtering. It is used for production of wear-resistant, corrosion-resistant and recently oxidation protection coatings of different materials in high temperature environments. Novel materials of interest for ultrahigh temperature structural applications are alloys in the system Mo-Si-B, as they show impressive oxidation resistance at high temperatures. In comparison to currently used Ni-based super alloys, operating temperatures with Mo-Si-B alloys can be increased beyond 1200°C. The Si to B ratio in the Mo-Si-B system strongly influences the oxidation resistance. Therefore, it is necessary to determine the exact composition of the coatings in order to control the production process and to ensure quality in application. For this purpose, different analytical methods are used, depending on the thickness of the coatings.

For analysis of coatings in the low micrometre range a new method, laser ablation inductively coupled plasma mass spectrometry (LA-ICP-MS), has been introduced recently. It is a versatile method which is applied for qualitative and semi-quantitative analysis in various fields of analytical chemistry. However, quantitative analysis represents a challenge of LA-ICP-MS. Non-stoichiometric effects, described as elemental fractionation, lead to differing composition of the ablated material compared to the composition within the sample. Moreover, the sample matrix strongly influences the ablation process, which means that the ablation rate of the same analyte is different in varying matrices. To overcome these problems, a commonly used but time-consuming method is calibration with matrix-matched standards. Additionally, for only a limited number of matrices commercially available certified reference materials can be used for calibration.

The goal of this work is the analysis of coatings with varying Mo, Si and B content deposited on an Al_2O_3 substrate by magnetron sputtering using LA-ICP-MS. Variation of the conditions during the deposition process leads to 12 different sample coatings with corresponding nominal concentrations, which serve as a reference. During this work three different calibration methods for LA-ICP-MS analysis are compared: one-point calibration, univariate calibration and multivariate calibration in the form of multiple linear regression.

Additionally, actual concentrations are determined using liquid ICP-OES analysis after sample digestion.

The results of one-point calibration indicate poor linear agreement, especially for Si. It is assumed that matrix effects play an important role during the ablation process and therefore influence the signal intensities and predicted concentrations. In order to further investigate the influence of matrix effects, the linear relationship between average signal intensities and the actual concentrations is tested. It is shown that no linear trend can be established, confirming the observations already made with one-point-calibration.

The samples exhibit differing contents of Mo, Si and B, which also means that their physical properties are strongly influenced. The absorption of the laser energy is different for each sample, which causes differing ablation rates and differing plasma load leading to non-comparable signal intensities and problems with matrix effects.

In this work it is presented that multivariate calibration can solve the problem of describing the complex dependence of the analyte concentration from the matrix without the need for matrix-matched standards. A multiple linear regression model is set up to predict the correlation between the concentrations determined by ICP-OES analysis and the signal intensities of the LA-ICP-MS measurement. Good linear agreement can be observed. Cross-validation and external validation confirm the reliability of the multivariate calibration model.

Kurzfassung

Physikalische Gasphasenabscheidung (PVD), welche ein Verfahren der Abscheidung von Dünnfilmen darstellt, wird in weitere Methoden unterteilt. Während der letzten Jahrzehnte hat sich besonders Magnetronsputtern für die Produktion verschleißbeständiger, korrosionsbeständiger, sowie zuletzt oxidationsbeständiger Beschichtungen verschiedener Materialien in Hochtemperaturumgebungen, durchgesetzt. Neue Materialien von Interesse für Hochtemperaturanwendungen sind Legierungen des Systems Mo-Si-B, da sie beeindruckende Oxidationsbeständigkeit bei hohen Temperaturen aufweisen. Im Vergleich zu gegenwärtig verwendeten Ni-basierenden Superlegierungen, können die Betriebstemperaturen mit Mo-Si-B Legierungen auf über 1200°C erhöht werden. Das Verhältnis Si zu B im Mo-Si-B System beeinflusst stark die Oxidationsbeständigkeit. Es ist daher notwendig die genaue Zusammensetzung der Beschichtungen zu bestimmen, um den Produktionsprozess zu kontrollieren und die Qualität in der Anwendung abzusichern. Zu diesem Zweck werden unterschiedliche analytische Methoden, in Abhängigkeit der Dicke der Beschichtungen, verwendet.

Für die Untersuchung von Beschichtungen mit Dicken im niedrigen Mikrometerbereich, wurde kürzlich eine neue Methode, Laserablation-Massenspektrometrie mit induktiv gekoppeltem Plasma (LA-ICP-MS), eingesetzt. Es ist eine vielfältige Methode, die für qualitative und semi-quantitative Analyse in verschiedenen Bereichen der analytischen Chemie eingesetzt wird. Allerdings stellt quantitative Analyse eine Herausforderung von LA-ICP-MS dar. Nicht-stöchiometrische Effekte, sogenannte Fraktionierungseffekte, führen zu abweichender Zusammensetzung des ablatierten Materials gegenüber der Zusammensetzung der Probe. Außerdem beeinflusst die Probenmatrix erheblich den Ablationsprozess. Die Ablationsrate eines Analyten ist unterschiedlich, je nachdem um welche Matrix es sich handelt. Um diese Probleme zu umgehen, werden für die Kalibration gewöhnlich matrix-angepasste Standards verwendet. Zusätzlich können nur für eine limitierte Anzahl an Matrices auch kommerziell verfügbare, zertifizierte Referenzmaterialien erworben werden.

Das Ziel der Arbeit ist die Analyse von Schichten mit variierendem Mo-, Si-, und B-Gehalt mittels LA-ICP-MS. Die Schichten werden auf einem Substrat aus Al_2O_3 mittels Magnetron-

sputtern abgeschieden. Änderung der Bedingungen beim Beschichtungsprozess ergibt 12 verschiedene Proben mit zugehörigen nominellen Konzentrationen, welche als Referenz dienen. In dieser Arbeit werden drei verschiedene Kalibrationsmethoden verglichen: Ein-Punkt-Kalibration, univariate Kalibration und multivariate Kalibration in Form von multipler linearer Regression. Zusätzlich wurden tatsächliche Konzentrationen mittels ICP-OES Analyse nach Aufschluss der Proben bestimmt. Die Ergebnisse der Ein-Punkt-Kalibration zeigen geringen linearen Zusammenhang, vor allem für Si, an. Man nimmt an, dass Matrixeffekte eine große Rolle während des Ablationsprozesses spielen und dadurch die Signalintensitäten und die bestimmten Konzentrationen beeinflussen. Um den Einfluss durch Matrixeffekte genauer zu untersuchen, wurde auf Linearität zwischen den durchschnittlichen Signal-intensitäten und den tatsächlichen Konzentrationen geprüft. Man kann zeigen, dass kein linearer Trend vorliegt, was die Beobachtungen der Ein-Punkt-Kalibration bestätigt.
Die Proben weisen unterschiedliche Gehalte an Mo, Si und B auf, was ebenfalls bedeutet, dass deren physikalische Eigenschaften stark beeinflusst werden. Die Absorption der Laserenergie ist für jede Probe unterschiedlich, was zu unterschiedlichen Ablationsraten und „plasma loads“ führt und in weiterer Folge untereinander nicht vergleichbare Signalintensitäten und Probleme mit Matrixeffekten verursacht.

In dieser Arbeit wird präsentiert, dass multivariate Kalibration das Problem, den komplexen Zusammenhang der Analytkonzentration von der Matrix zu beschreiben, ohne die Notwendigkeit von matrix-angepassten Standards lösen kann. Zur Vorhersage des Zusammenhangs zwischen den bestimmten Konzentrationen (ICP-OES Analyse) und den mittels LA-ICP-MS erhaltenen Signalintensitäten, wird ein Modell mit Hilfe von multipler linearer Regression aufgestellt. Gute lineare Übereinstimmung kann erreicht werden. Kreuzvalidierung und externe Validierung bestätigen die Verlässlichkeit des multivariaten Kalibrationsmodells.

Table of contents

Acknowledgement

First of all I want to thank my supervisor Andreas Limbeck for the possibility to do my Master's thesis in his group, for his great support throughout my work, and for always finding the right words to keep me going in hard times. He always let me know that he thinks highly of me as a student and member of this group, and I am deeply grateful for that.
In this regard my thanks also go to Maximilian Bonta, who immensely helped me with the data analysis and was always ready to give me advice. His indestructible optimism and mindfulness have contributed to my appreciation of him not only as a mentor, but also as a friend.

I want to express my gratitude to the group of Prof. Paul Heinz Mayrhofer (Department of Materials Science, Vienna University of Technology), mainly Annika Vieweg and Helmut Riedl, for the great cooperation. Many thanks go to Johannes Frank for his support in our work.

A big thank you to all members of the group for good scientific ideas and for fun lunch breaks together. A very special thanks goes to Victoria Mohr who has become a major part of my life. She understands the life of a scientist, a friend, a runner and she has always been there, throughout ups and downs in every part of our lives.

To my close friends, Ana-Marija Brkic, Gordana Maric, Alexander Kadnar, Sabine Eder, as well as Tobias Zolles, Elke Ludwig, Julia Firmkranz, Marlene Wallnberger, Gloria Winkler and Monika Bi, who have known me for very long and have accompanied me on my way, I want to say thank you. They enrich my life in every possible way. I am grateful for my friend Yee Ann Ho and her amazing family, for treasuring our friendship through letters travelling the world. I also want to thank the 'Sieger der Herzen'-group.

I am deeply grateful for my friend Ronan Cullen, for his love, his support, and for making my life complete.

Finally, I want to thank my wonderful family with all my heart for their love, their support, and for helping me to make the right choices, my sister Tina Cakara for seeing into my soul and my cousin Petra Vida for her trust.

1. Introduction

The application of materials in oxidative, and in particular in high temperature, environments represents a major challenge in terms of oxidation resistance. To extend the lifetime of the materials and to maintain the desired properties, it is necessary to provide oxidation protection by deposition of coatings on the material surface. Thus, in many fields of science and technology the use of thin metal or ceramic coatings is of increasing importance [1, 2].

The deposition process of thin coatings is realised by various techniques [3], however, magnetron sputtering has gained importance over the last decades and has become the method of choice for many industrial applications, such as the manufacturing of hard, wear-resistant coatings, and corrosion-resistant coatings [4]. Furthermore, magnetron sputtering is applied for the production of oxidation protection coatings of different materials in high temperature environments [5, 6]. Recently, the materials of interest for ultrahigh temperature structural applications are alloys in the system Mo-Si-B [7]. In comparison to currently used Ni-based superalloys, which show limitations due to their melting points, the operating temperatures can be increased beyond 1200°C when using Mo-Si-B alloys [8]. Molybdenum as a refractory metal offers the advantage of a high melting point, and thus good mechanical strength and creep resistance. Boron doped molybdenum silicide alloys show impressive oxidation resistance at high temperatures, as a protective borosilicate layer is formed, which functions as an oxygen diffusion barrier [8]. At temperatures between 400 and 800°C, however, extreme oxidation, commonly known as pesting, takes place [9]. The problem of pesting can be overcome by very fast heating-up below 1000°C and application of the material only at high temperatures, for instance as it is implemented in gas turbines [7]. It is known that the Si to B ratio in the Mo-Si-B system strongly influences the oxidation resistance. By increasing the Si content, the oxidation resistance at high temperatures is enhanced due to formation of a protective SiO_2-rich layer [10]. In contrast, higher boron content leads to improvement of the oxidation resistance within the pesting region. Another problem, which occurs above 1200°C, is the loss of material on account of the high volatility of B_2O_3. Hence, the successful usage of Mo-Si-B alloys for high temperature applications calls for control and minimisation of oxidation processes, which can be realised by means of protective coatings. The complex issue of oxidation resistance and its impact on coating

designs has been described by Pint *et al.* [11]. The main aspects to be considered, apart from oxidation resistance at high temperatures, are a good thermal expansion match and chemical compatibility between the coating and the substrate, and the problem of interdiffusion, which limits the lifetime of the protection.

Sakidja *et al*. [12] proposed a coating design for Mo-Si-B alloys meeting the requirements mentioned above. Packed aluminium reacts with Mo to form an oxidation resistant coating. Additionally a protective Al_2O_3 layer is produced on the surface under oxygen exposure.

Mo-Si-B based materials can provide oxidation protection for other substrates, such as SiC-C composites, which are promising materials for ultrahigh temperature applications due to their low density [13]. The coating material is compatible to the substrate because of their matching thermal expansions. Furthermore, no interdiffusion between the two materials was observed.

Recently, a coating strategy using magnetron sputtering for deposition has been reported [7], with the substrate as well as the coating consisting of Mo-Si-B based materials. Oxygen diffusion barriers are needed to achieve long-term stability of the system.

To control the production process and to ensure quality in application analytical methods which offer sensitive and rapid characterisation of coatings with high spatial resolution are necessary. Depending on the thickness of the layers different methods are applied for the characterisation. Secondary ion mass spectrometry (SIMS), X-ray photoelectron spectroscopy (XPS) and auger electron spectroscopy (AES) for example are mainly applied for surface investigations, however, can be used for analysis of thin layers up to tens of nanometres [14]. Quantitative depth profiling analysis of coatings over the wide range of several nanometres to hundred micrometres thickness is carried out by means of glow discharge optical emission spectrometry (GD-OES) [14, 15]. Fast and accurate quantification combined with high depth resolution and the possibility of multi-element analyses are advantages of this technique. Furthermore, the use of a radiofrequency (rf) instead of a direct current (dc) discharge source for the sputtering process allows for the analysis of non-conducting materials [16]. Another method, where the glow discharge process is coupled with mass spectrometry (GDMS), offers increased sensitivity and isotopic information if compared to optical spectrometry techniques. GDMS can be used in pulsed operation mode, which offers the possibility of time-resolved measurements to overcome the problem of

interferences mainly caused by the discharge gas [17]. Pulsed GD is often performed in combination with time-of-flight MS as reported, for example, by Pisonero et *al.* [18], since the GD pulse can easily be synchronised with the detection time, thus leading to high analyte signals temporally separated from interferences. In general, the temporal and spatial separation of the atomisation and ionisation processes in GD techniques results in low matrix-dependence and therefore in easy quantification without the need for matrix-matched calibration [19]. All techniques mentioned above are suitable for the analysis of very thin layers, however, measurements of coatings in the micrometre range are time-consuming. The need for low-pressure working conditions represents another disadvantage of SIMS and GD techniques.

For depth profiling of micrometre thick layers a new method, laser ablation inductively coupled plasma mass spectrometry (LA-ICP-MS), has been introduced recently. Interaction of a pulsed laser with the sample material causes ablation of the material creating small particles, which are subsequently transported to the inductively coupled plasma by a carrier gas. In contrast to GD and SIMS, laser ablation ICP-MS can be operated at ambient pressure and allows for very fast analysis.

The possibility to analyse insoluble or poorly soluble materials, samples with no specific requirements on shape or dimension, and conducting as well as non-conducting samples of different structure are additional benefits of laser ablation [20]. Apart from that, it is considered to be a quasi non-destructive method which is particularly important in forensic chemical analysis or archaeology [21]. The wide dynamic range and the high sensitivity of the ICP-MS are advantages that, coupled with LA, allow for multi-element analysis of major, minor, and trace elements as well as isotope ratio measurements [22].

The diameter of the laser beam usually varies between some µm to hundreds of µm and depending on the application can be adjusted to the needs of the user. The adjusted laser beam diameter results in a slightly increased diameter of the ablation spot on the sample surface, which means that the actual resolution is decreased due to thermal effects.

Typical laser ablation systems with nanosecond long pulse durations show restricted spatial resolution due to thermal effects and thereby the analysis is limited to the micrometre

range. For various applications, however, ns-LA-ICP-MS offers sufficient resolution and allows for the analysis of coatings in the range of several micrometres.

Analysis of layers with depth resolution in the submicrometre range is usually achieved by fs-LA-ICP-MS, which is a promising method for depth profiling [23]. The capabilities of fs-LA-ICP-MS for investigation of thin metal coatings have been studied by Pisonero *et al.* [20]. Another approach for depth profiling of very thin layers involves adjustment of the laser power and the focal position for the ablation process [24], allowing the use of nanosecond LA systems. Focusing the laser beam above the surface of the solid sample, instead of focusing it directly onto the surface, and reducing the laser energy leads to an ablation pit of decreased depth that is larger in diameter. The lower energy density, however, causes reduction of the amount of ablated material, which in particular has an effect on the determination of trace analytes.

The following examples show the capabilities of ns-LA-ICP-MS for depth profiling in various fields.

Depth profiling studies of ZrTiN hard ceramic coatings deposited by PVD were carried out by Kanický *et al.* [14]. It has been shown that qualitative depth profiling of the 3 µm-thick coatings is possible and that optimum measuring conditions strongly depend on the dimensions of the ablation cell as well as the pit diameter. For the investigations an ArF* 193-nm excimer laser ablation system with a beam homogeniser has been used.

In archaeological applications mainly the advantage of LA-ICP-MS to obtain isotopic information is utilised. Combined with the possibility to analyse thin layers, it represents a fast analytical tool for the determination of the origin of archaeological discoveries. The characterisation of a glazed layer on antique ceramics is reported in the work of Resano *et al.* [25].

Another field of interest is the appliance of depth profiling in forensic chemistry using LA-ICP-MS, such as the analysis of car paints in crime investigations. Car paints are applied as a multilayer coating of about 100 µm thickness in total [26]. The elemental composition of the individual layers helps to discriminate different paints of the same colour and attribute them to the specific cars. The forensic chemical analysis of document paper and inks is another interesting application for measurements of micrometre thick layers. Trejos *et al.* [27]

showed that the elemental composition of paper and ink varies with different brands and different manufacturing sites and makes it possible to distinguish between them.

Qualitative and semi-quantitative analysis using LA-ICP-MS are applied in various fields of analytical chemistry, however, for a wide range of samples quantitative analysis is a challenge and represents a major limitation of the method. The sample matrix strongly influences the ablation process, which means that the ablation rate of the same analyte is different in varying matrices. Non-stoichiometric effects, described as elemental fractionation, occur in all laser-based techniques and lead to differing composition of the ablated material compared to the composition within the sample and display a limitation of LA-ICP-MS [22]. Fractionation can occur during the ablation process due to element dependence and their properties, laser wavelength and crater morphology [28]. Moreover, fractionation can occur during the aerosol transport, as well as the ionisation process inside the plasma flame, and is mainly dependent on the particle size distribution of the ablated particles.

For calibration and quantitative analysis by LA-ICP-MS different methods are applied. One approach is the use of commercially available certified reference materials. However, certified reference materials are limited to a small number of matrices and are usually costly in their purchase. Hence, external calibration with matrix-matched standards is the most commonly used calibration method in order to obtain accurate results [28].

In this work a LA-ICP-MS method for quantitative analysis of Mo, Si and B in thin oxidation resistant coatings for ultrahigh temperature applications has been developed. The exact concentrations of Mo, Si and B of different samples were determined by ICP-OES after sample preparation in the form of digestion with acids. Additionally, LA-ICP-MS analysis of the solid samples was carried out. For quantitative analysis three different calibration methods, namely one-point calibration, univariate calibration, and multivariate calibration, were compared. Moreover, the influence of matrix effects on the calibration methods was investigated.

2. Theoretical aspects

2.1 Inductively coupled plasma optical emission spectrometry (ICP-OES)

2.1.1 Sample introduction

Different techniques are used for the analysis of liquid and solid samples by ICP-OES. Conventional sample introduction allows for the analysis of solutions and liquids. A nebuliser disperses the solution into a fine aerosol, which is then introduced into the plasma flame. Larger droplets are removed by means of a spray chamber before entering the plasma. Direct introduction techniques for solid samples include electrothermal vaporisation (ETV) and laser ablation (LA). [29]

2.1.2 Sample excitation and optical emission

The sample aerosol is transported by a carrier gas and enters the inductively coupled plasma through an injector tube, which is placed in the middle of the plasma torch. The quartz torch consists of three concentric tubes: the inner tube (injector tube) for the introduction of the sample through the carrier gas flow, the intermediate tube, serving as a supplier for auxiliary gas, and the outer tube, where coolant gas is introduced tangentially to the intermediate tube. Typically argon is used for the gas supply of carrier, auxiliary, and coolant gas. The coolant gas maintains the plasma and is usually introduced at a flow rate of about 15 L min^{-1}. Carrier and auxiliary gas are operated at lower flow rates of approx. 1 L min^{-1}.

The top section of the torch is surrounded by a water-cooled copper coil, which is connected to a radio frequency (rf) generator. A high frequency (HF) electromagnetic field, used for ignition and maintenance of the plasma, is induced into the coil by the rf generator. For ignition of the plasma a high-voltage spark is applied. It leads to the formation of free electrons, which are accelerated in the electromagnetic field, causing ionisation of argon atoms by collision. The formed ions interact with further argon atoms in a chain reaction and generate more and more atoms until a plasma is formed. The temperature of the plasma reaches 6 000 – 10 000 K at operating conditions depending on the energy of the electromagnetic field and the applied gas flows. Within the plasma the temperature decreases constantly towards the tail plume, being the highest in the region close to the coil.

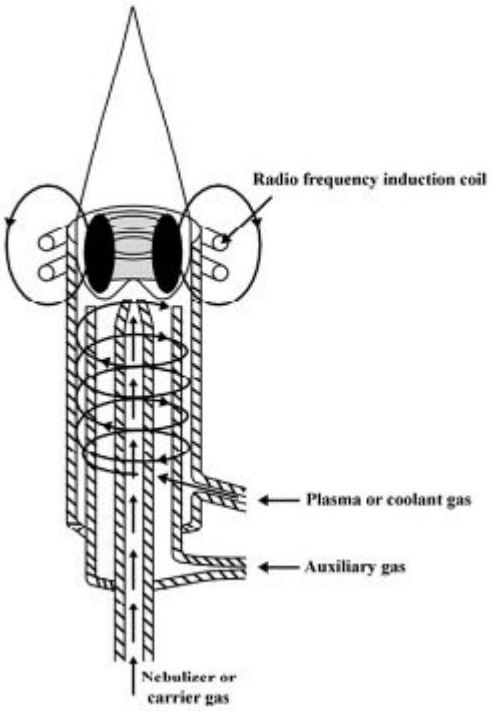

Figure 1 Schematic view of the plasma torch in radial observation mode [30]

When the sample aerosol in form of liquid droplets enters the plasma different processes take place. The first step is desolvation into a dry aerosol, which is followed by vaporisation to a gas and dissociation of the gas into atoms. In the last step simultaneous excitation and ionisation of the atoms occurs. The excited atoms lead to emission of radiation in the UV and visible spectral range, when falling back to the ground-state. In ICP-OES the analytical procedure is based on the measurement of the emitted radiation. [29]

2.1.3 Optical dispersion and detection

The emitted radiation enters the optical system through a ceramic cone next to the plasma flame and is subsequently dispersed according to its wavelength. For the dispersion process two possible optical arrangements are applied, the Czerny-Turner type and the echelle grating-based monochromator. The Czerny-Turner type monochromator disperses the entering radiation by means of an optical grating. In this work an optical system based on echelle grating was used, which is shown in Figure 2. The dispersion process takes place in two steps. In the first step the incident light is dispersed into different orders of diffraction by the echelle grating. In the second step dispersion into single wavelengths is achieved by a prism, generating a spectrum in two dimensions which is projected onto the charge injection

device (CID) detector. The detector helps to provide qualitative information, which is obtained through the dispersion process, as well as quantitative information by measuring the intensity of the radiation. [29]

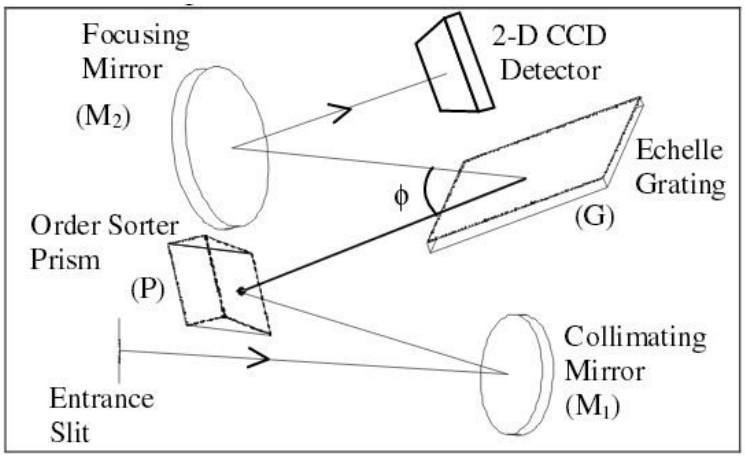

Figure 2 Schematic view of an echelle optical system [31]

2.2 Inductively coupled plasma mass spectrometry (ICP-MS)

Inductively coupled plasma mass spectrometry (ICP-MS) is a multi-element analytical technique used in a wide range of applications, such as environmental, biological, industrial, and archaeological analyses. Multi-element capability, a wide dynamic range, and high sensitivity, as well as the possibility to obtain isotopic information are the main advantages of this technique. The dynamic concentration range in ICP-MS instruments reaches up to 12 orders of magnitude and, depending on the analysed elements, detection limits at the low ppt (= pg/L) range are achieved when liquid sampling is used [32].

2.2.1 Sample introduction

For sample introduction of liquid samples a nebuliser generates a fine aerosol, which is then introduced into the plasma. Commonly used solid sample introduction systems are ETV and laser ablation, which will be described in more detail later.

2.2.2 Sample ionisation in the plasma

The principles of the plasma generation and the processes inside the plasma are comparable to the ones of the ICP-OES technique described above. In contrast to ICP-OES, usually the

axial viewing mode is used to take advantage of the longer viewing path and thus a higher sensitivity. Compared to ICP-OES, where the emitted radiation is used to obtain analytical information, in ICP-MS the generated ions are of further interest. The ionisation efficiency depends on the first ionisation potential of the elements. The higher the first ionisation potential, the lower is the percentage of ionised atoms. Alkali and alkaline metals achieve a degree of ionisation of more than 99 %, most metals more than 90 % and non-metals, such as Cl and B, for less than 5 % of the atoms ionisation takes place [32], thus leading to high efficiencies when alkali or alkaline metals are analysed and low ionisation efficiencies of non-metallic compounds. [33]

2.2.3 Ion extraction interface

Ionisation inside the plasma takes place under atmospheric pressure, however, ion separation and detection are performed under high vacuum conditions, with pressures below 10^{-5} mbar [32]. The extraction of ions from the plasma is therefore carried out through a two-stage vacuum interface consisting of two metal cones (Figure 3). Both cones are usually composed of nickel, or in special cases of platinum, and have small round openings with a diameter of about 1mm for the sample cone and a smaller diameter for the skimmer cone. The sample cone is arranged in direct contact with the plasma and is used for the extraction of the plasma, which expands into a gas jet within the lower pressure region between the cones. In the second step the central part of the jet enters the skimmer cone and transfers it to the high vacuum region. [33]

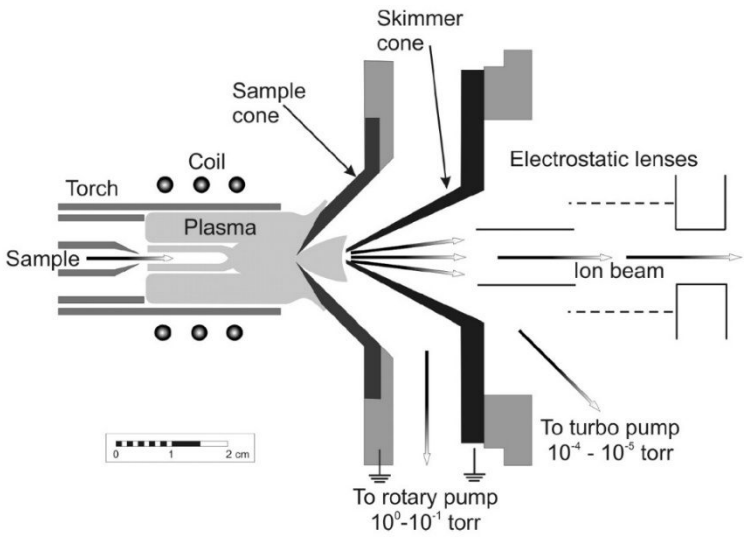

Figure 3 Typical two-stage ion extraction interface [34]

2.2.4 Ion focussing and transport

In order to reach the mass analyser, ions have to be focused and transported using ion optics in form of electrostatic lenses, each with a specific voltage. The focussing of the ion beam through electrostatic lenses is shown in Figure 3. The transport efficiency depends on the applied lens voltages, which have a different effect on ions with different mass. Optimisation of lens voltages is usually performed to achieve maximum sensitivity for elements in the middle of the mass range, but decreased sensitivity for heavy and light isotopes. Additionally the space-charge effect, caused by the mutual repulsion of ions within the ion beam, leads to expansion of the beam and thus deflection of lighter ions. Hence, focussing of the ion beam is necessary for improved transport to the analyser.

Apart from ion focussing, the ion optics have another important use. When the gas jet emerges from the interface region it does not only contain ions, but also photons and neutral species, which have to be separated before they enter the detector, otherwise the detection sensitivity would be affected. Photons and neutrals are separated by placing a metallic disk, known as photon stop, in between the plasma and the detector. Applying a voltage to the disk leads to deflection of ions, while neutrals and photons are stopped. [33]

2.2.5 Ion separation and detection

Separation of ions from the ion beam is achieved by the means of a mass analyser, which differentiates ions based on their mass-to-charge-ratio (m/z). There are different types of mass spectrometers used in ICP-MS. The most common one is the quadrupole mass analyser, which was used in the following experiments. The analyser consists of four metal rods, on which differing voltages are applied. The metal rods are arranged in such a way that opposite rods have the same electrical charge. Applied voltages cause entering ions to oscillate inside the quadrupole, allowing only ions with resonance frequency to pass the quadrupole in a stable path. Only ions with a specific m/z ratio show resonance, other ions are deflected and discharged at the metal rods. By stepwise changing of the applied voltages, the m/z ratio of the ions which pass the quadrupole is varied and leads to sequential scanning of the whole mass spectrum in a time scale of about 100 ms.

Other commercially available devices include sectorfield and time-of-flight (ToF) mass spectrometers. Compared to quadrupole mass spectrometers, sectorfield devices offer

lower scan speed but higher mass resolutions, allowing for resolution of differences in m/z down to 0.01-0.001 mass units. The great advantage of ToF devices is the possibility for simultaneous detection of the whole mass spectrum.

Ions separated by the mass analyser reach the detector and are counted by converting each ion into a discrete electrical pulse. The number of pulses can be then correlated to a concentration. Pulse counting detectors use electron multiplication for signal enhancement. Each ion hits the dynode and causes emission of secondary electrons, which hit the dynode to form more electrons in a chain reaction leading to multiplication of the signal. [33]

2.3 Laser ablation

Laser ablation (LA) as a solid sampling technique for ICP-MS analysis was first introduced in 1985 [35]. Since then effort has been made to further develop and improve this technique. Reduced sample preparation time, no specific requirements on sample size, as well as structure and composition of the sample, and the possibility of spatially resolved analyses are advantages of laser ablation, which offer an alternative to sampling through solution nebulisation. Today laser ablation represents a widely applicable solid sampling technique, which, combined with ICP-MS, allows for highly sensitive multielement analysis and isotope ratio measurements. Figure 4 presents a schematic view of a typical LA-ICP-MS arrangement. [21]

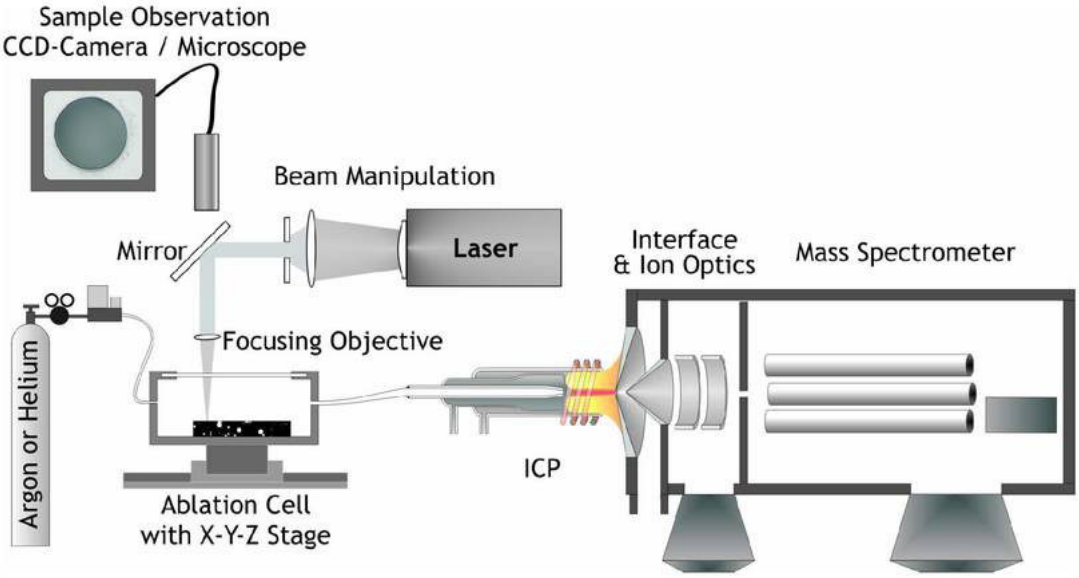

Figure 4 Schematic view of a laser ablation system coupled to ICP-MS [22]

The principle of the laser ablation process is based on the interaction of a pulsed laser focused on the sample surface, which absorbs the laser energy. Absorption of the energy leads to processes involving melting, vaporisation, atomisation and ionisation of the sample, as well as generation of sample particles of different size, with dimensions ranging from nanometer to micrometer. The emerging material plume expands, forming a local plasma. The complex mechanisms of particle formation are known to be material-dependent among other things, however, are not yet fully understood. [36]

Furthermore, the processes occurring during laser ablation are strongly influenced by two characteristics, the laser wavelength and the laser pulse duration. Shorter wavelengths result in higher photon energy, better ablation rate, lower fractionation and better precision. The second aspect, being the laser pulse duration, is based on the duration of fundamental processes within the sample material happening in the picosecond (ps) time scale (e.g. lattice vibrations of atoms). Commonly used lasers work with laser pulses in the nanosecond (ns) time scale. Recently effort has been made to develop and improve ablation systems by application of lasers with femtosecond (fs) long pulse durations, which offer certain advantages compared to ns-laser ablation. [21]

Three principle types of lasers have been used for laser ablation of solid materials: ruby, Nd:YAG and excimer lasers. Ruby lasers with wavelengths in the visible light range were applied at the beginning of LA-ICP-MS as an analytical method. Relatively affordable price, robustness, easy operation and wide wavelength range (fundamental wavelength 1064 nm in the IR range, down to 213 nm in the UV range through optical frequency quintupling) are advantages which nowadays make solid state Nd:YAG lasers the most commonly used source for laser ablation. Excimer lasers use halogens as operating gas which determines the laser wavelength, for instance ArF-excimer with a wavelength of 193 nm in the low UV range is widely used. The use of UV lasers has recently gained in importance due to the advantages of better focus and higher absorption of UV radiation by the sample material when compared to lasers using IR or visible radiation. [28]

The ablation stage consists of a lens, an ablation chamber, where the sample is placed, and an adjustable platform, which allows exact positioning of the sample. Usually the sample surface is viewed remotely by a CCD camera through the fused silica window of the ablation chamber. For analyses using laser ablation coupled with ICP-MS, the air tight ablation

chamber is flushed with an inert gas, typically argon or helium, in order to transport the ablated particles to the ICP.
The typical set-up of a laser ablation system, consisting of the laser and the ablation stage, is shown in Figure 3.

LA-ICP-MS is considered to be a very useful and versatile technique for direct analysis of solid samples, yet there are several limitations that need to be mentioned. Non-stoichiometric, matrix-dependent effects, described as elemental fractionation, lead to a differing composition of the ablated material compared to the composition in the sample, thereby limiting accurate quantitative analysis. Additionally, the ablation behaviour and the ablation rate of an analyte is strongly dependent on the sample matrix. [28]
To a large extent these problems can be overcome with the use of matrix-matched calibration, which, however, often requires in-house matrix matching, as the availability of certified reference materials is very limited.
Another approach to decrease fractionation effects is the application of fs-laser ablation. As already mentioned in this section, the laser pulse duration plays an important role during the ablation process. When nanosecond long laser pulses are used, the time range is long enough for absorption of energy in the material surrounding the laser spot through thermal diffusion causing the “heat-affected zone”. Further damages caused by the interacton of the ns long laser pulse with the material include generation of microcracks, recast material, redeposition of ablated material and damage in adjacent structures. As a consequence of the “heat-affected zone”, fractionation effects, particularly due to redistribution of material, can occur. In contrast, for fs-LA the pulse duration falls below the ps-time range, meaning insufficient time for thermal diffusion into the surrounding material. Hence, no thermal effects and less collateral damage are observed, which can eliminate fractionation effects and matrix dependence. Moreover, fs-LA generates smaller particles and more uniform particle size distributions, leading to decreased fractionation affects. The possibility to overcome the limitations of ns-LA-ICP-MS by using a shorter laser pulse, however, is associated with high costs. [37]

2.4 Multivariate calibration

Quantitative analysis in analytical chemistry usually requires calibration methods in order to describe the relationship between the interesting variable and the measured (input) variables. In most cases the use of univariate calibration, for instance in form of simple linear regression, is sufficient to describe the relationship of one measured, independent variable and the interesting, dependent variable.

However, some analytical techniques presuppose the use of multivariate calibration due to the complicated relationship between interesting and input variables [38]. In comparison to univariate calibration, in multivariate calibration methods the interesting variable depends on more than one input variable.

In order to perform accurate quantitative analysis using either univariate or multivariate calibration, a calibration model needs to be set up, which predicts the relationship between the variables. Various methods for model design are applied in analytical chemistry. For univariate data analysis, as already mentioned above, simple linear regression models are used to describe the relationship between dependent and independent variable. In multivariate calibration different approaches exist for model design. More important methods include multiple linear regression (MLR), partial least squares regression (PLS) and principal component analysis (PCA). Figure 5 shows a schematic view of the basic concept of multivariate calibration. [39]

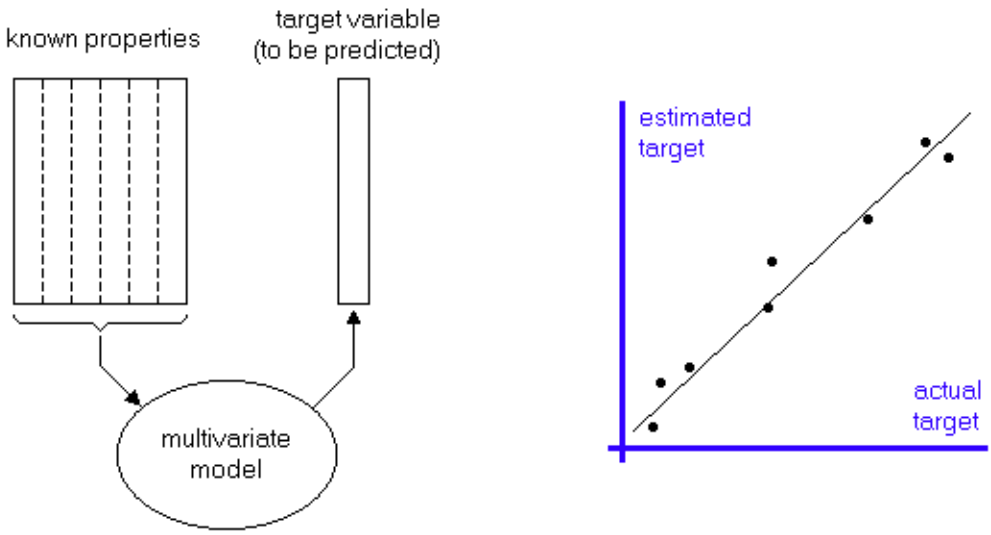

Figure 5 Schematic view of the basic concept of multivariate calibration [39]

In this work a multiple linear regression (MLR) model was used for multivariate calibration. The following linear equation describes the relationship between the target variable y and n input variables x_i based on the MLR model:

$$y = ß_0 + ß_1x_1 + ß_2x_2 + \dots + ß_nx_n + \varepsilon$$

where y denotes the dependent or response variable, $x_1 – x_n$ denote the n independent or predictor variables and $ß_0$ - $ß_n$ are the regression coefficients. This model describes a hyperplane in the n-dimensional space. The parameter $ß_0$ represents the intercept of the regression plane. The parameter $ß_i$ represents the expected change of the response variable y per unit change in x_i when all of the remaining response variables are held constant. [40]

Creating a calibration model from a finite amount of data includes a small chance that the model does not describe the underlying relationship in an accurate way, but is caused by random effects. This problem mainly occurs in the case of non-linear or complex models, which need validation methods in order to confirm the reliability of the model. Decreasing number of measurements and increasing number of variables increase the chance of invalid models. In contrast, some linear multivariate calibration methods, such as MLR, provide theoretical foundation on the estimation of the reliability of a calibration model. Thus, additional validation is not necessarily required, as the reliability is tested during the calculation process and can be expressed by means of theoretical values such as F-values.
Notwithstanding, in this work an internal validation method called cross-validation or “leave-one-out” method was applied to additionally test the reliability of the calibration model. The idea of cross-validation is based on splitting the model data into two data sets, including a larger one, which represents the “training set”, and a smaller one, which is here described as “test set”. The training set is used to set up the model and the test set validates the model by applying the model to the test set. The obtained results are then compared to the expected values, which are defined in the test set. This procedure is repeated with the complete model data, gradually defining new training and test sets in order to validate every object of the data set. The deviation of the results obtained by cross-validation from the expected values is expressed in the form of the PRESS value (see below). [39]

The size of the test set is variable, depending on the needs of the user, however, the usual approach is definition of only one data object for the test set, the rest of the data generates the training set. This approach is also called full cross-validation or leave-one-out-cross-validation.

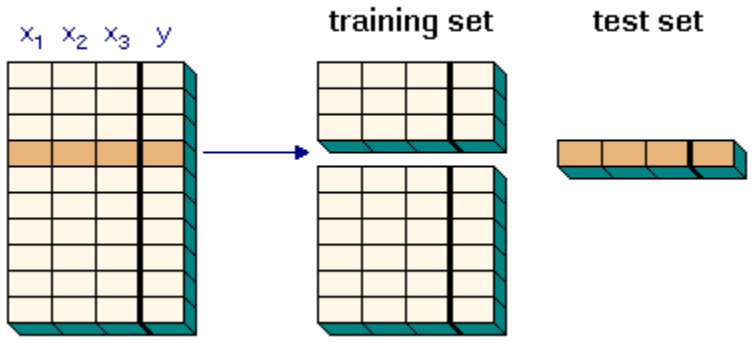

Figure 6 Basic concept of cross validation [39]

The performance of the model is determined by calculation of the PRESS (predictive error sum of squares) value. In multivariate statistics the specification of degrees of freedom and calculation of the standard error is not always possible. In order to evaluate the prediction error of the calibration, the PRESS value, which describes the quadratic mean of the observed residuals, is used:

$$RMSEP = \sqrt{\frac{PRESS}{n}} = \sqrt{\frac{\Sigma\,(y_i - y_i^*)^2}{n}}$$

RMSEP stands for “root mean squared error of prediction” and is calculated by summing all squared prediction errors of cross-validation. RMSEP describes the reliability and the predictive ability of a calibration model, low RMSEP values indicating good predictive ability of the model. RMSEP is used to specify the reliability of a calibration model for internal as well as external validation. Hence, the RMSEP can also be referred to as RMSECV (root mean squared error of cross-validation). [39]

External validation of a multivariate calibration model is another validation method. A certain number of samples within an experiment is analysed and used for the creation of a

calibration model. The model is then applied to the rest of the samples and the obtained results are verified by comparison with the expected results. Hence, external validation is mainly useful when the model is applied for quantitative analysis of further samples, either of the same experiment or additional sets of experiments. In the latter case external validation represents an essential aspect for the application of a calibration model, for example in routine analyses.

Setting up a multivariate calibration model is usually associated with a large number of independent variables x_i. In order to determine which variables contribute to the explanation of the response variable y, they have to be tested and selected. The selection process is based on finding the best model fit, which contains as little variables as possible.
Several approaches are used for variable selection, which mainly depend on the type of the model. For linear regression models usually stepwise procedures are applied, including forward selection, backward selection and stepwise regression. In this work the selection of variables was carried out by means of stepwise regression, which is a special case of forward selection. The basic principle of forward selection is selecting the independent variable, which offers the best fit for the dependent variable y, and then stepwise increasing the number of variables until a stop criterion is met. For linear regression usually partial F values are used to set the limits for the stepwise selection process, thereby defining the stop criterion. Stepwise regression follows the same idea as the forward selection algorithm, however, additionally to the stepwise selection, each time a new variable is added, all selected variables are tested for significant contribution to the calibration model. If the contribution is not significant, the variables in question are eliminated. This means that also previously selected variables can be eliminated, and therefore the obtained variables can differ from the ones evaluated by forward selection. At the beginning of the stepwise regression algorithm the correlations between all the independent variables x_i and the dependent variable y are calculated. The variable with the highest correlation is used as the starting variable. Afterwards the variable with the highest partial F-value is added and all variables are checked for their partial F-values, eliminating the variables that fall below a predefined threshold. The procedure is repeated by stepwise addition of new variables until a stop criterion is met. [39]

3. Experimental

3.1 Reagents

All reagents used in this work were of analytical grade or higher purity levels. Concentrated nitric acid and concentrated hydrofluoric acid were purchased from Merck, Germany and Applichem, Germany, respectively. Commercially available 1000 mg L^{-1} Indium stock solution in 2 % v/v HNO_3 (TraceCERT, Fluka, Switzerland) was used as an internal standard by dilution with 1% v/v HNO_3. Calibration standards were prepared by dilution of 10 mg L^{-1} ICP MS Calibration Standard 4 stock solution in H_2O tr. HF (VWR, USA). All solutions were prepared with high purity water obtained from an Easypure II water system (Thermo Scientific, USA) with a conductivity of 18 MΩ cm^{-1}.

3.2 Instrumentation

Measurements by conventional liquid sampling were performed on an iCAP 6500 ICP-OES spectrometer (Thermo Scientific, USA) in combination with a CETAC ASX-520 autosampler (CETAC technologies, USA). The ICP-OES device is presented in Figure 7. A peristaltic pump with a 2 bridges PVC tube (inner diameter of 1.02 mm) was used for transport of the sample solution to the ICP-OES. The HF resistant sample introduction system consisted of a PEEK Mira Mist nebuliser (Burgener Research Inc., Canada), a PTFE spray chamber, and a plasma torch with a ceramic injector tube of 1.5 mm inner diameter. For data acquisition iTEVA software (Thermo Scientific, USA) was employed and the recorded emission signals were background-corrected. Laser ablation measurements were carried out on a quadrupole ICP-MS Thermo iCAPQc (ThermoFisher Scientific, Germany) instrument. For data acquisition Qtegra software (v. 1.5.1189.31) was employed. An image of the ICP-MS device is shown in Figure 8.

Figure 7 Thermo Scientific iCAP 6500 ICP-OES spectrometer used for the performed experiments [41]

Figure 8 ThermoFisher Scientific quadrupole ICP-MS iCAPQ instrument employed for the performed experiments [42]

For solid sampling a laser ablation system with a frequency quintupled 213 nm Nd:YAG laser source (NWR213, New Wave, ESI, USA) was coupled to the ICP-MS. The high performance ablation chamber with 100mm x 100mm dimensions was used to locate the samples. An approximately one metre long tube with an inner diameter of 2 mm served as the connection between the ablation chamber and the ICP-MS. The helium carrier gas stream was mixed with argon gas through a tee-piece connector before entering the plasma.

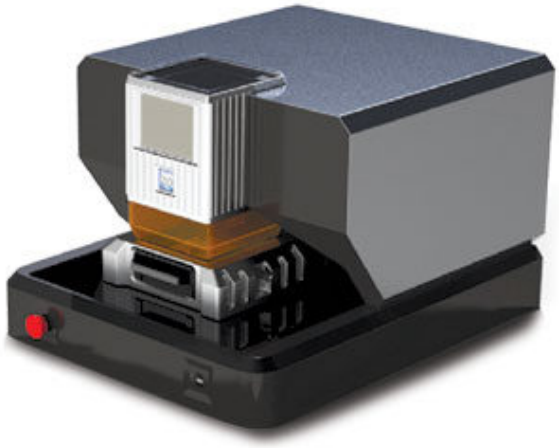

Figure 9 New Wave, ESI 213 nm Nd:YAG laser source used for the performed experiments [43]

Microscopic images of the ablation craters were viewed using an Olympus BX60 microscope. Recording of the images was carried out by means of Infinity Analyze software (Release 6.0, Lumenera Corporation).

3.3 Preparation of coatings

Coatings with varying B, Mo and Si content deposited on an Al_2O_3 substrate by magnetron sputtering were used as samples. Sputtering is a physical vapour deposition (PVD) process, which bases on the fact that atoms are ejected from a solid target through physical processes, such as collision processes with bombarding argon ions. Usually DC (direct current) diode sputtering systems are used for the deposition process, where the target material is operated as the cathode and the substrate as the anode. The deposition chamber is filled with a working gas, in this case Ar, which is ionised due to the applied DC voltage generating a visible plasma through glow discharge. The Ar^+ ions are accelerated onto the cathode and eject atoms from the target material.

The deposition rate can be increased by placing a magnetic arrangement behind the cathode, which causes an overlap between the electrical and magnetic field and thereby the electrons to get trapped over the target in the form of a closed loop. The trapping of the electrons leads to an increased collision rate of the electrons with Ar gas molecules. More Ar ions are formed, which eject more atoms from the target material, thus increasing the

deposition rate on the substrate. This type of sputtering process is called magnetron sputtering.

The deposition process was carried out on an AJA Orion5 Lab scale magnetron sputtering system, using a target configuration with three separate elementary targets of B, Mo and Si. The molybdenum target was operated with a DC signal obtained from a DC generator (AJA DCXS power supply). Due to charging effects of the target material and subsequent isolation of the cathode, difficulties occur when non-conducting materials are used as sputtering targets. Thus, the silicon and boron target were operated by a DC pulsed plasma generator (ENI PRG-100). The pulsed DC signal allows for the emerging charge to flow off during the off-pulse. The deposition process was performed in pure Ar atmosphere at a working pressure of 10^{-2} mbar and at a substrate temperature of 500°C. More details regarding the sputtering mechanism and the deposition process can be found in the diploma thesis of Annika Vieweg [44].

3.4 Sample preparation and liquid ICP-OES analysis

The samples were broken into pieces of approximately 2 mm in diameter and 4 replicates underwent the preparation process. To dissolve the coating, digestion with concentrated acids was carried out in sterile, metal-free centrifuge tubes (Polypropylene, VWR, USA). 2 mL HNO_3 and 0.25 mL HF were added to the sample pieces, the tubes were shaken vigorously, heated in a boiling water bath for several minutes and allowed to stand overnight at ambient temperature. The centrifuge tubes remained closed throughout the digestion procedure to avoid evaporation of volatile compounds. The obtained solutions were diluted to 45 mL with high purity water containing about 2% v/v HNO_3 and 0.3% v/v HF and stored at 4°C until further usage. For accurate determination of the Mo content, it was necessary to further dilute several samples in a ratio of 1:5 or 1:10 using high purity water (2% v/v HNO_3 and 0.3% v/v HF).

Operating parameters for the liquid ICP-OES analysis are given in Table 1. Background-corrected emission signals were recorded with an analysis time of 5 s and 5 repeats per sample. External calibration was used for quantification and Indium with a concentration of 1.5 mg L^{-1} served as an internal standard. After every four samples, control standards and reagent blanks were analysed for quality control.

Table 1 ICP-OES operating parameters

RF generator power	1200 W		
Auxiliary gas flow	0.8 L min^{-1}		
Nebuliser gas flow	0.6 L min^{-1}		
Coolant gas flow	12 L min^{-1}		
Radial viewing height	11 mm		
Max. integration times	6 s		
Solution uptake rate	0.8 mL min^{-1}		
Analytical wavelengths (nm)			
B	208.893	249.773	
Mo	202.030	204.598	281.615
Si	250.690	288.158	

3.5 LA-ICP-MS analysis

Samples were fixed on glass slides using double sided tape and placed into the ablation chamber, which was purged with He carrier gas at 1 L min^{-1} for about 15 minutes before the start of a measurement. For optimisation of the ICP-MS operating parameters, the maximum signal intensity of ^{115}In in NIST 612 trace metals in glass standard (National Institute of Standards and Technologies, USA) was set before the analysis. Transient (time resolved) signals consisting of a 10 s long background signal and line scans with a duration of approximately 50 s for ablation of the material were recorded. For data analysis background-corrected average signal intensities were evaluated by setting 5 regions with duration of 6 s within the constant transient signals.

After each measurement spot scans with duration of 30 s were recorded to fully remove the coating and to ablate the substrate material. Based on the assumption that the substrate has the same composition for each sample, the recorded ^{27}Al-signal was used for normalisation.

All samples were analysed in standard mode. Operating parameters for the laser ablation process, as well as the ICP-MS measurement are given in Table 2.

Table 2 LA-ICP-MS operating parameters

Laser ablation system	
Average fluence	7.9 J cm^{-2}
Laser diameter	150 µm
Scan speed	75 µm s^{-1}
Repetition rate	5 Hz
Carrier gas flow (He)	0.75 L min^{-1}
ICP-MS system	
RF power	1550 W
Nebuliser gas flow	0.8 L min^{-1}
Auxiliary gas flow	0.8 L min^{-1}
Cool gas flow	14 L min^{-1}
Dwell time	0.01 s
Measured isotopes	^{10}B, ^{11}B, ^{27}Al, ^{28}Si, ^{29}Si, ^{30}Si, ^{44}Ca, ^{48}Ti, ^{76}Se, ^{94}Mo, ^{95}Mo, ^{100}Mo, ^{108}Pd, ^{114}Cd, ^{138}Ba, ^{184}W

3.6 Data analysis

Multivariate calibration in form of stepwise multiple linear regression was performed with the programme DataLab version 3.5 for statistical data analysis

4. Results and discussion

The samples used in this work were coatings of 2-3 µm thickness with varying Mo, Si and B content, deposited on an Al_2O_3 substrate by magnetron sputtering. The temperature and pressure settings during the deposition, as well as the composition of the target materials, influence the final composition of the deposited material. Modification of the settings during the sputtering process resulted in 12 different samples with varying nominal concentrations of Mo, Si and B, which are presented in Table 3. Samples containing all three components exhibit good oxidation resistance for structural applications at ultrahigh temperatures, as well as within the pesting region (400 and 800°C), where usually extreme oxidation occurs. For comparison, samples containing no boron (sample 1 and 12) and no silicon (sample 5) were analysed in order to investigate the effect on the properties of the material and the composition accordingly.

Table 3 Nominal concentrations of Mo, Si and B (in weight %) in ascending order of the Mo content. The sum of the concentrations of every compound equals to 100%.

	concentration / wt%		
Sample number	**Mo**	**Si**	**B**
1	77.35	22.65	0.00
2	81.99	14.32	3.69
3	83.73	14.60	1.67
4	86.49	11.92	1.59
5	89.87	0.00	10.13
6	89.94	6.69	3.38
7	90.61	5.31	4.08
8	94.91	4.96	0.13
9	95.10	4.64	0.26
10	98.03	1.85	0.12
11	98.22	1.55	0.24
12	99.41	0.59	0.00

4.1 ICP-OES analysis

The first experiments performed in this work comprised sample preparation and ICP-OES analysis of the obtained sample solutions. The sample preparation as described in the experimental section included digestion with concentrated HNO_3 and HF in 4-fold replicate of each sample, dilution with high purity water, as well as further dilution for the determination of the Mo content. External calibration in the linear concentration range (0 ppm to 3 ppm) was used for quantification and Indium with a concentration of 1.5 mg L^{-1} served as an internal standard. Background-corrected emission signals were recorded with an analysis time of 5 s and 5 repeats per sample. For each element two or three analytical wavelengths were used for the determination of average concentrations (see Table 1). Additionally the concentrations of four replicate measurements were included in the calculation of the average concentrations, as well as the corresponding standard deviations and relative standard deviations (RSD).

Table 4 Measured average concentrations, standard deviations and relative standard deviations (RSD) of Mo, Si and B (in weight %) by ICP-OES analysis in corresponding order to Table 3. The sum of the concentrations of every compound equals to 100%.

	concentration / wt%			RSD / %		
Sample number	**Mo**	**Si**	**B**	**Mo**	**Si**	**B**
1	77.80 ± 0.07	22.20 ± 0.15	0.00	0.09	0.68	-
2	82.77 ± 0.63	14.99 ± 0.56	2.24 ± 0.07	0.76	3.74	3.13
3	81.58 ± 0.12	16.64 ± 0.17	1.78 ± 0.07	0.15	1.02	3.93
4	85.65 ± 0.27	13.33 ± 0.30	1.01 ± 0.05	0.32	2.25	4.95
5	95.90 ± 0.04	0.00	4.10 ± 0.04	0.04	-	0.98
6	89.40 ± 0.27	8.10 ± 0.16	2.50 ± 0.12	0.30	1.98	4.80
7	92.45 ± 0.51	4.30 ± 0.56	3.25 ± 0.07	0.55	13.0	2.15
8	94.32 ± 0.19	5.65 ± 0.18	0.12 ± 0.01	0.20	3.19	8.33
9	93.8 ± 0.28	5.95 ± 0.12	0.24 ± 0.02	0.30	2.02	8.33
10	97.45 ± 0.07	2.36 ± 0.06	0.2 ± 0.01	0.07	2.54	5.00
11	97.79 ± 0.07	1.97 ± 0.06	0.25 ± 0.02	0.07	3.06	8.00
12	99.51 ± 0.06	0.49 ± 0.06	0.00	0.06	12.2	-

Table 4 presents the average concentrations, standard deviations and RSDs for the ICP-OES analysis. For Mo excellent RSD values below 1% are achieved. RSDs of Si and B generally range between 1 and 5 %, however, increased RSD values are obtained at low Si or B contents.

Figures 10 - 12 show the correlation of the nominal concentrations given by the deposition process and the measured concentrations by ICP-OES as presented in Table 3 and Table 4. The solid line (x=y) denotes agreement between nominal and measured concentration for each sample. The vertical error bars indicate the standard deviation of the measured average concentrations determined by ICP-OES measurement as presented in Table 4.

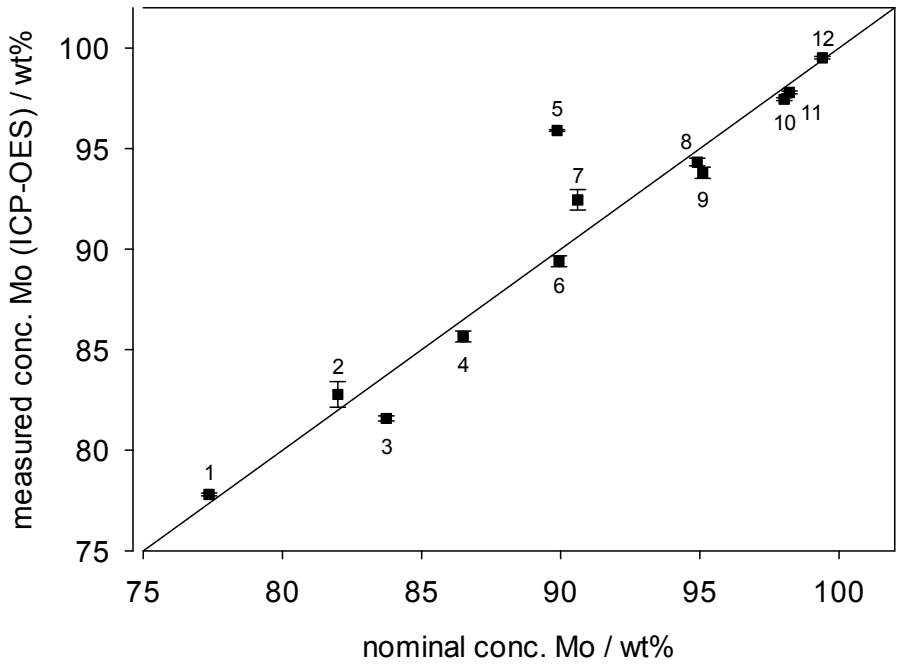

Figure 10 Measured concentrations (in weight %) of (a) Mo and (b) Si as a function of the nominal concentrations given by the settings during the deposition process

Nominal and measured concentrations for Mo are in general agreement, however, concentrations of most of the samples differ from the desired values around 1-2 wt%. Generally there is slight under-determination of Mo, which can correlate to the over-determination of Si in Figure 11. Samples exhibiting higher measured than nominal concentrations, such as samples 5 and 7, can be associated with the under-determination of B (see below).

The measured concentrations of Si (Figure 11) differ from the nominal concentrations about 1-2 wt%, which is comparable to the results already obtained for Mo. There is a general trend for over-determination of Si.

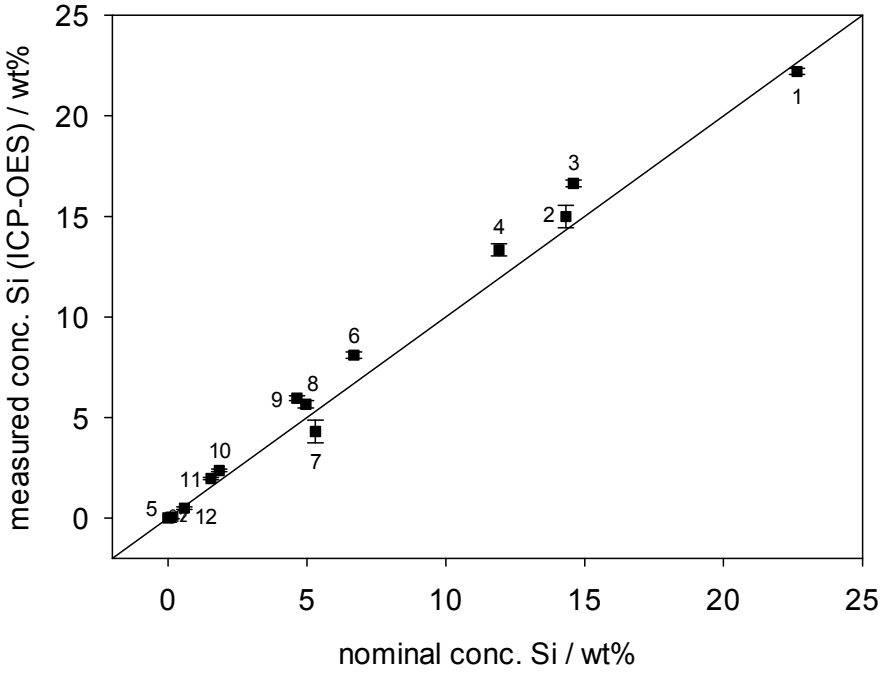

Figure 11 Measured concentrations (in weight %) of (a) Mo and (b) Si as a function of the nominal concentrations given by the settings during the deposition process

Figure 12 shows the correlation of measured and nominal concentrations for boron. An observation we would like to point out is the under-determination of B, especially at concentrations above 3 wt% (samples 2 and 5-7). It is assumed that the variation in boron content is influenced by the magnetron sputtering process and is not due to the ICP-OES measurement. Sample number 5 exhibits a deviation of the boron concentration in the order of 6 wt%, when compared to the nominal concentration. This is probably due to the fact that silicon is not present in the sample and the processes during the deposition of the coating are influenced, leading to considerably lower boron contents. However, further investigations are needed to back up this assumption, as no samples were produced in this work which contain Mo, Si and B, and additionally have a boron content of 10 wt% or above. High contents of boron lead to improvement of the oxidation resistance of the coating material within the pesting region, however, it also means decreased oxidation resistance at

high application temperatures. Therefore, from the material science point of view, coatings with boron contents of about 10 wt% are not suitable for high temperature applications in any case.

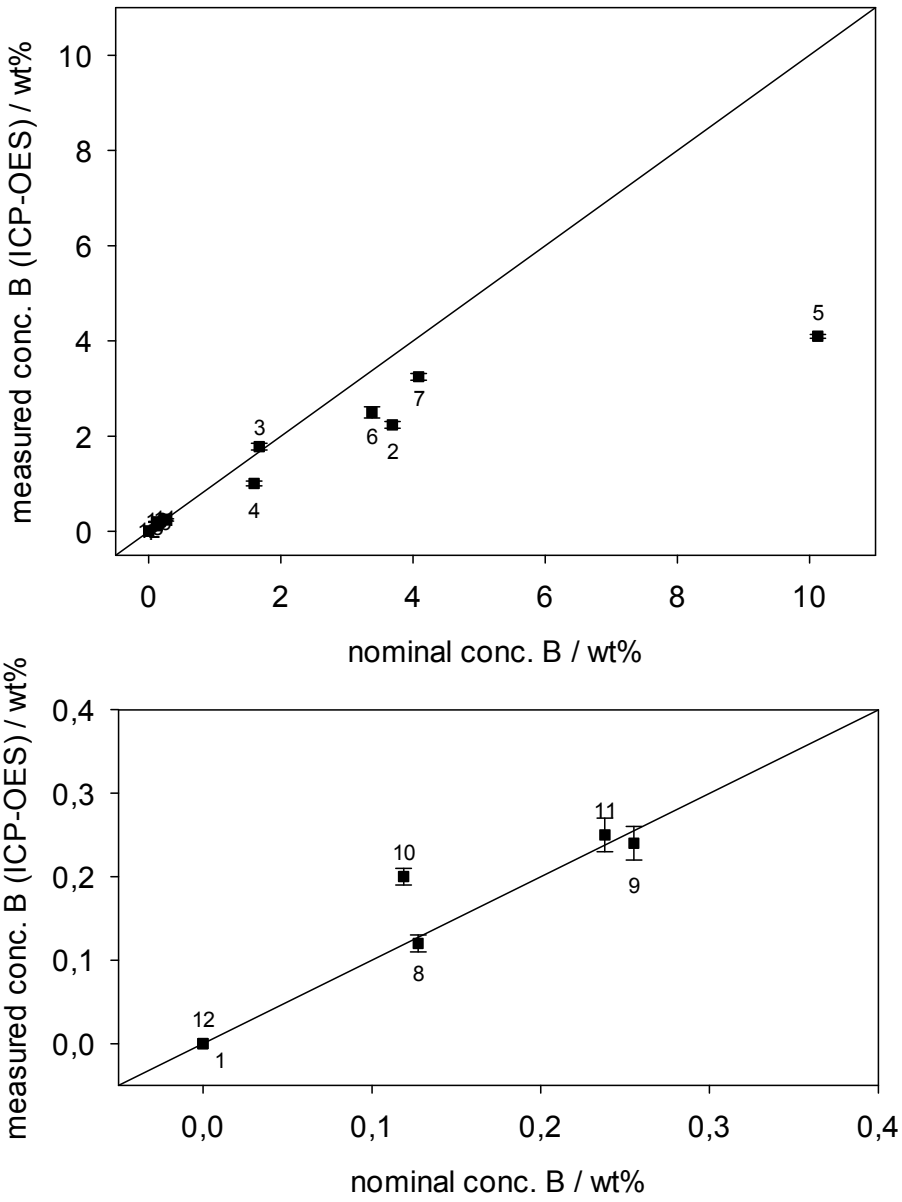

Figure 12 Measured concentrations (in weight %) of B as a function of the nominal concentrations given by the settings during the deposition process; concentrations between 0 wt% and 0.4 wt% are additionally zoomed in

4.2 LA-ICP-MS analysis

Apart from ICP-OES analysis of the sample solutions, measurements of the solid samples by LA-ICP-MS were carried out to circumvent the sample preparation process. Transient (time resolved) signals consisting of a 10 s long background signal and line scans with a duration of LA-ICP-MS were carried out to circumvent the sample preparation process. Transient (time resolved) signals consisting of a 10 s long background signal and line scans with a duration of approximately 50 s for ablation of the material were recorded. The pulsed laser moved with a scan speed of 75 µm s^{-1} and a repetition rate of 5 Hz, ablating material in the form of a line with a diameter of 150 µm. Interaction of the laser with the sample leads to formation of a crater on the sample surface, where the material got ablated. Figure 13 presents a range of the used samples, each containing the ablation craters formed by a line scan and the magnification of one sample displayed in the image on the right-hand side. Further measurement parameters for the LA-ICP-MS analysis are shown in Table 2.

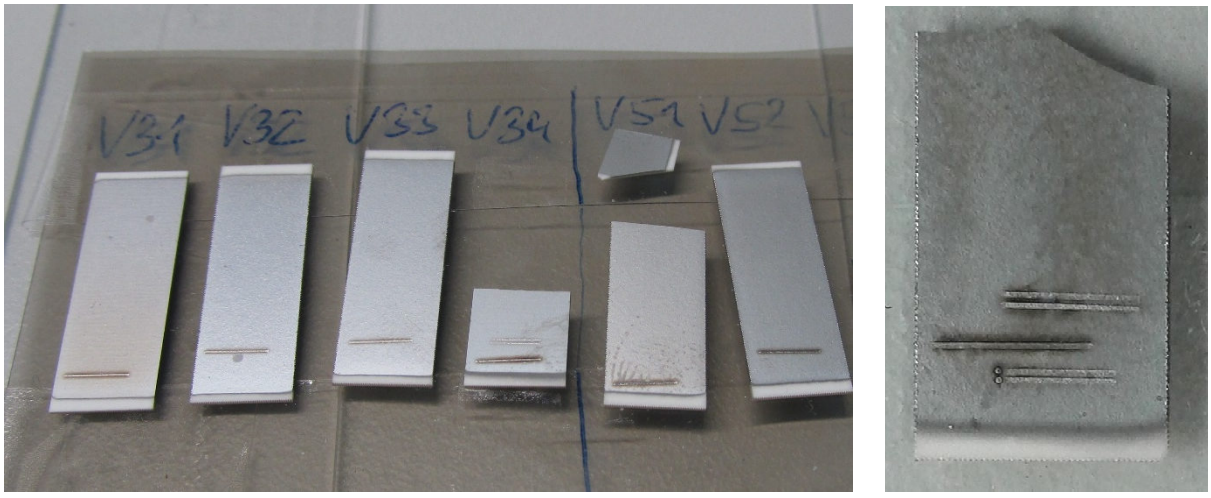

Figure 13 Ablation craters generated by line scans during the laser ablation process

For all samples transient signal intensities were recorded using LA-ICP-MS. Background-corrected average intensities of 5 constant transient signal regions were evaluated, each with a 6 s time interval. Figure 14 shows the results of the transient measurement for sample 2 for all measured elements, where the logarithmic signal intensities of the analytes (in counts per second) are illustrated as a function of the time (in s). The baseline which is recorded at the beginning of the measurement was used for background-correction. The

signal regions are marked in green colour. Constant signal intensities are provided throughout the transient measurement, indicating homogeneous sample coatings.

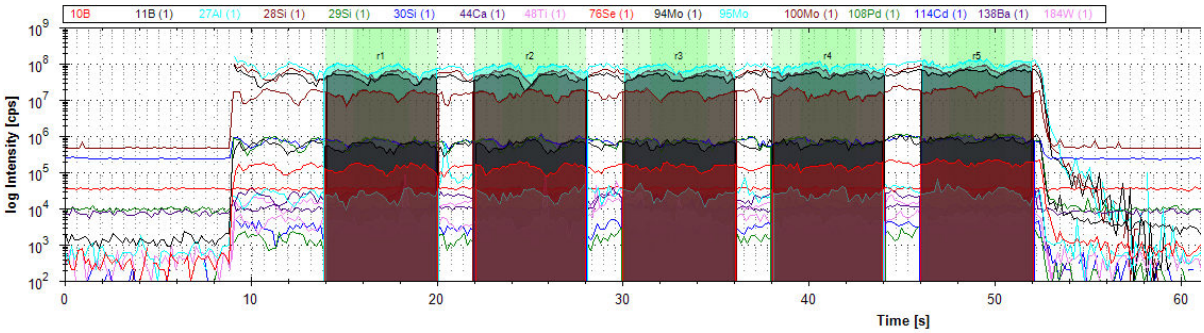

Figure 14 Example for a transient measurement using LA-ICP-MS (sample 2)

4.2.1 One-point calibration

Quantitative analysis represents one of the major challenges for laser ablation as a solid sampling technique in analytical chemistry [28]. The basic approach is the use of one-point calibration, which means that a sample serves as a reference sample. For calibration ideally certified reference materials or matrix-matched standards are used in order to minimise matrix effects. However, certified reference materials are limited to a small number of matrices and matrix-matching usually involves complex and time-consuming preparation before the analysis. Therefore, in order to overcome difficulties related to matrix-matching, in this work one of the samples coatings served as the reference sample. Sample number 2 was chosen as the reference sample due to the fact that coatings of given composition feature the best properties considering oxidation resistance. Moreover, the sample includes all three analytes, which concentrations are located approximately in the middle of the concentration range of the measured samples.

Figures 15-17 show the predicted concentrations based on the LA-ICP-MS analysis of Mo, Si and B (in weight %) as a function of measured concentrations by ICP-OES analysis. The vertical error bars indicate the standard deviation of the predicted concentration resulting from 5 replicate transient signal regions. The solid line (x=y) denotes agreement between nominal and predicted concentration for each sample. Relative deviations with a threshold of 10 % were defined, as they represent good agreement when solid sampling methods are used.

It can be observed that relative deviations for Mo are within the limits of 10 % across the entire concentration range and general deviations are up to 5 %. As Mo is the main component of the coating, relative deviations are within the limits by trend. Variation in concentration of Mo by several percent only influences the relative deviation marginally. Therefore, the linear correlation between measured and predicted concentration is insufficient for this work, as the determination of the accurate concentrations plays an important role for the physical properties of the material and for reliability in application.

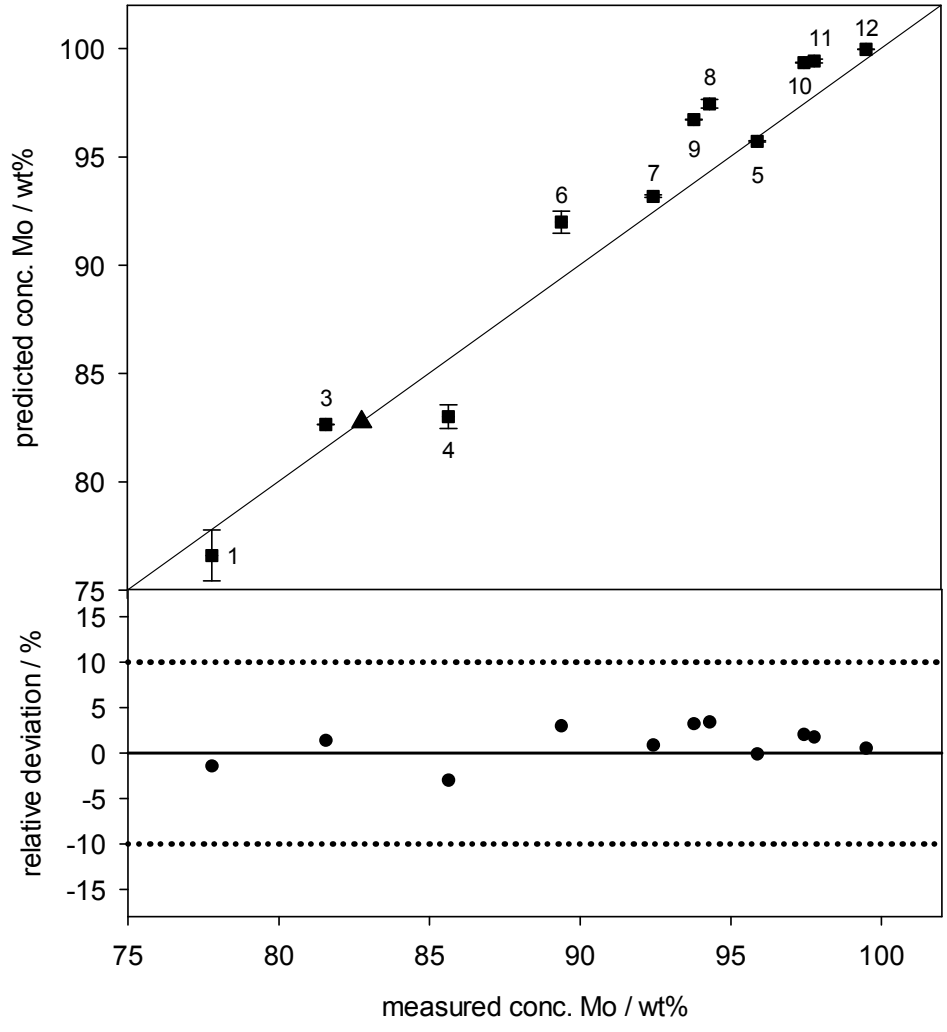

Figure 15 Concentrations of Mo predicted by LA-ICP-MS analysis as a function of the measured concentrations by ICP-OES analysis. Relative deviations (in %) of the predicted concentrations from the measured concentrations, the dashed lines mark the 10% limit. The triangular symbol indicates the reference sample.

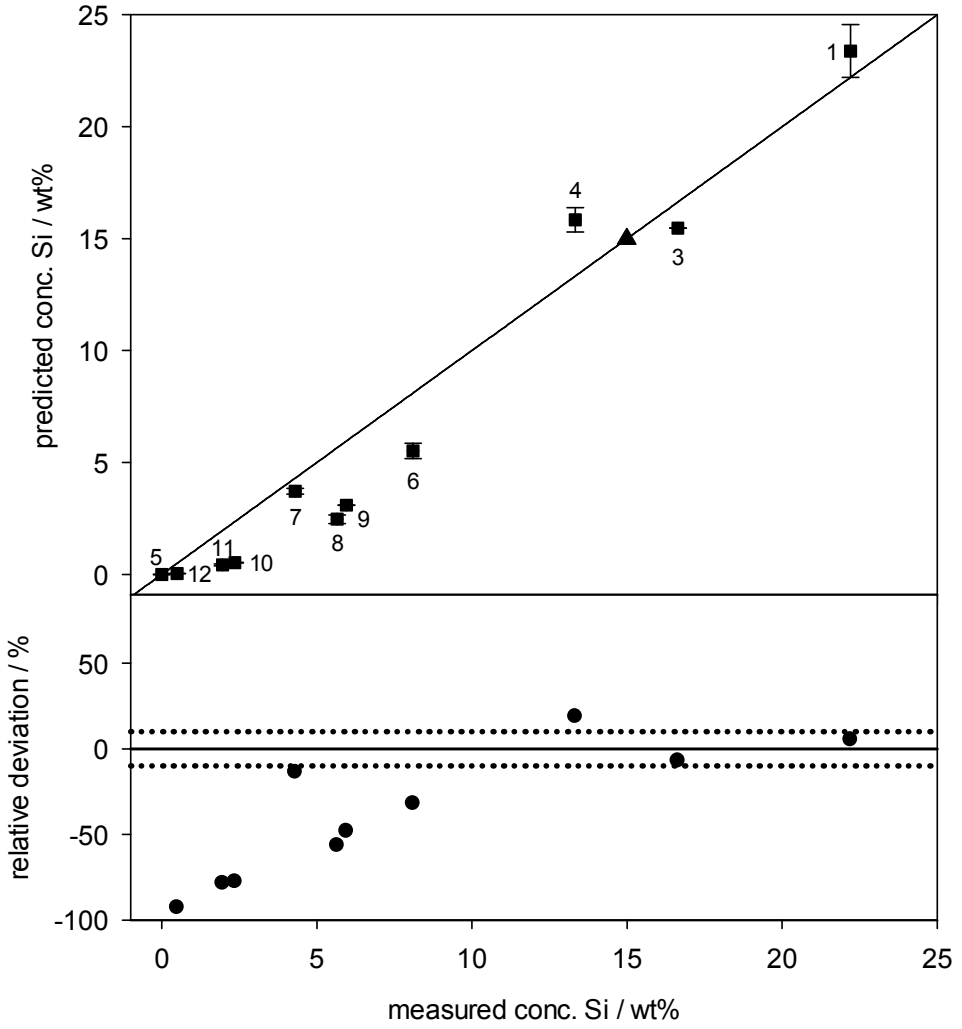

Figure 16 Concentrations of Si predicted by LA-ICP-MS analysis as a function of the measured concentrations by ICP-OES analysis. Relative deviations (in %) of the predicted concentrations from the measured concentrations, the dashed lines mark the 10% limit. The triangular symbol indicates the reference sample.

Figure 16 shows the correlation between measured (ICP-OES analysis) and predicted (LA-ICP-MS analysis) concentration for Si. Relative deviations for seven samples lie higher than the 10 % limit. Samples with Si concentrations up to 3 wt% exhibit deviations close to 100 % and samples in the concentration range between 5 and 10 wt% around 50 %. Moreover, a distinct trend for under-determination of Si below concentrations of 10 wt% can be observed.

Figure 17 presents the results of one-point calibration for boron. Samples with boron contents below 0.5 wt% exhibit relative deviations between 20 and 40 %. This is due to the fact that the concentrations of B are very low compared to the content of Si and Mo in the same samples and relative deviations for concentrations close to 0 usually have higher deviations. Standard deviations of the samples with B concentrations above 1 wt% are within the 10 % limit.

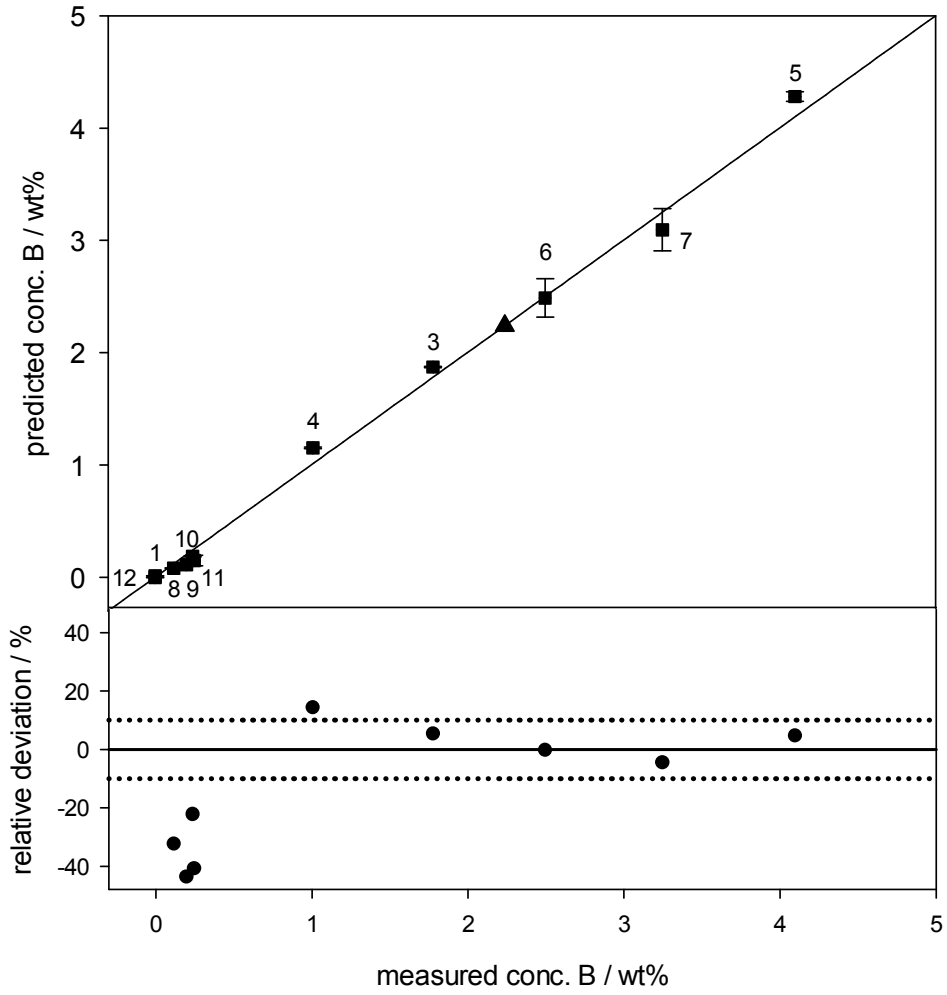

Figure 17 Concentrations of B predicted by LA-ICP-MS analysis as a function of the measured concentrations by ICP-OES analysis. Relative deviations (in %) of the predicted concentrations from the measured concentrations, the dashed lines mark the 10% limit. The triangular symbol indicates the reference sample.

4.2.2 Univariate calibration

One-point calibration showed that the predicted concentrations, especially for silicon, differed from the measured concentrations when only one standard was used as reference. It was demonstrated that the relative deviations of Si for are higher than 10 % for most of the samples and that a trend for under-determination can be observed. Relative deviations of Mo and B are within the limit, however, one-point-calibration is not a method which is accurate enough for quantitative analysis using LA-ICP-MS in this work. The samples among each other exhibit different ablation behaviour and ionisation efficiencies inside the plasma. In order to consider that, it is necessary to use more than one standard for calibration. The precondition is linear relationship between the measured concentrations and the average signal intensities from the LA-ICP-MS analysis.

Figure 18 and 19 present the average signal intensities of the LA-ICP-MS measurement as a function of the measured concentrations obtained by ICP-OES analysis. The vertical error bars indicate the standard deviation of the average signal intensities obtained from the LA-ICP-MS measurement resulting from 5 replicate transient signal regions. The horizontal error bars indicate the standard deviation of the measured average concentrations determined by ICP-OES measurement as presented in Table 4. There is no linear correlation between the average signal intensities and the measured concentrations for all three components.

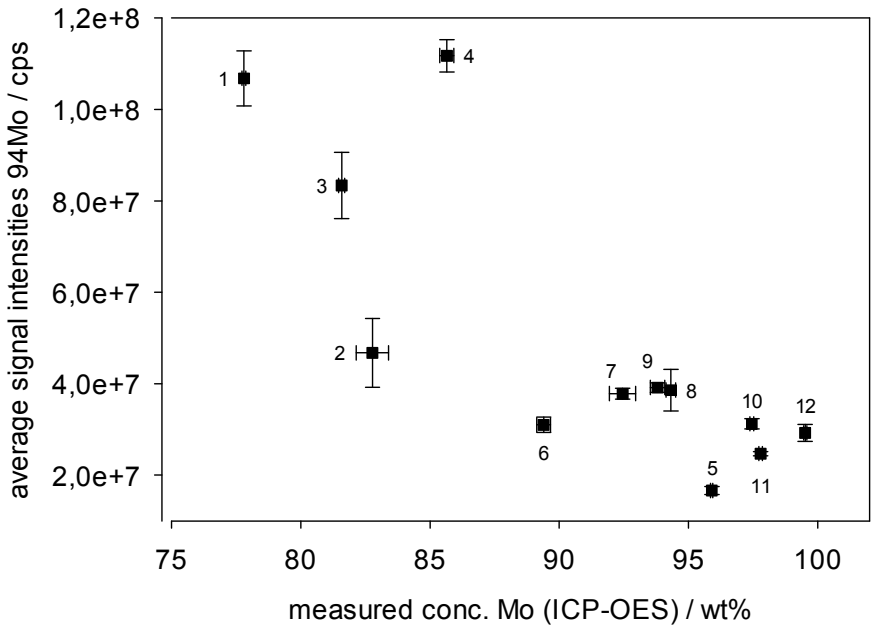

Figure 18 Average signal intensities (in counts per second) of Mo obtained by LA-ICP-MS analysis as a function of the measured concentrations given by the ICP-OES analysis

For Mo no linear relationship can be established due to the fact that the highest signal intensities are obtained at concentrations between 75 and 85 wt%, which is the opposite of the observations made for Si and B. Moreover, concentrations ranging between 90 and 100 wt% exhibit similar signal intensities and show no change with increasing concentration.

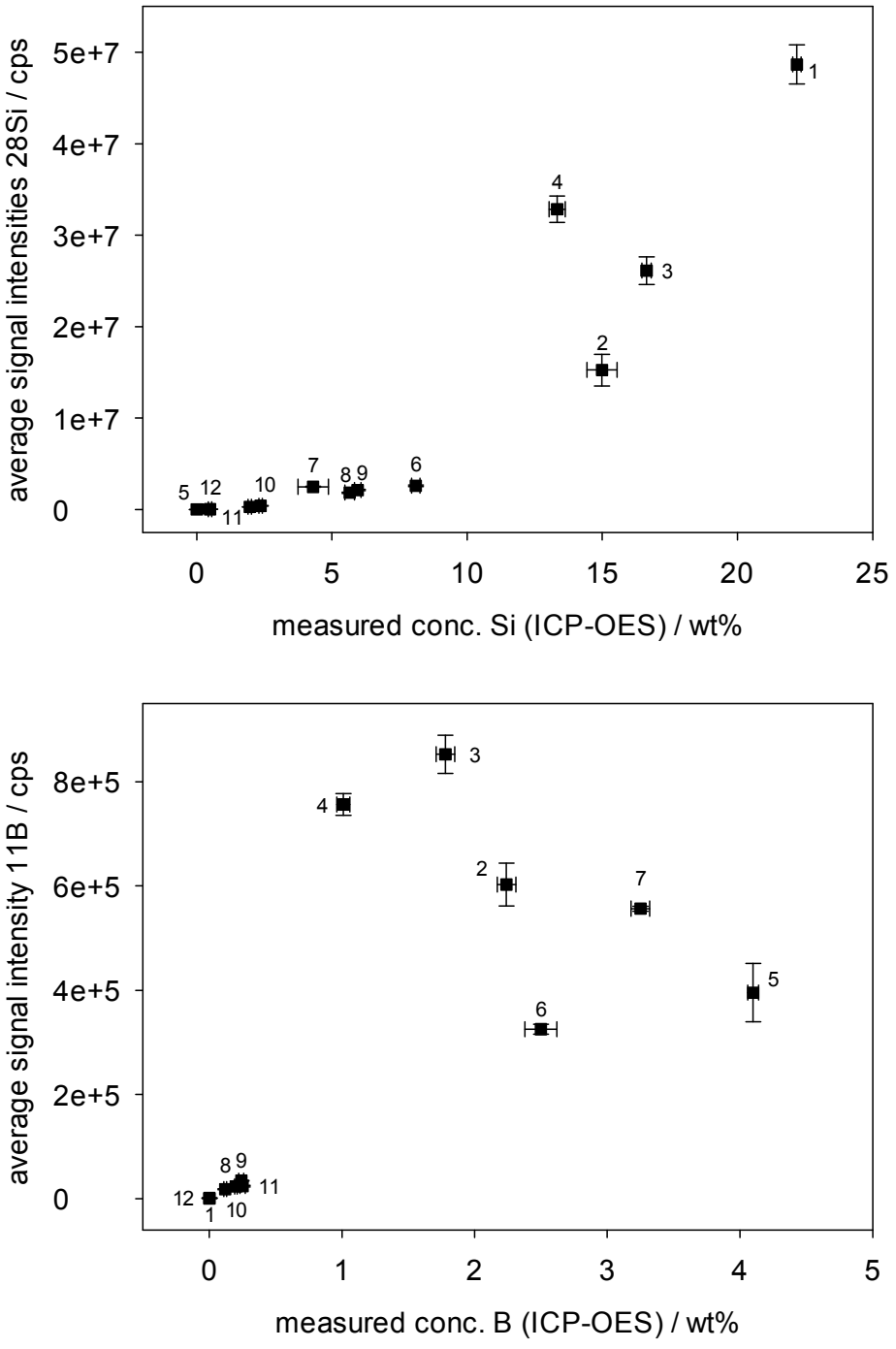

Figure 19 Average signal intensities (in counts per second) of (a) Si and (b) B obtained by LA-ICP-MS analysis as a function of the measured concentrations given by the ICP-OES analysis

Signal intensities associated with silicon concentrations below 10 wt% stay at the same level and no increase with concentration can be observed. This is in agreement with the results obtained by one-point calibration. It was suggested that the under-determination of Si can be attributed to the laser ablation process and that the signal intensities are influenced by matrix effects.

Figure 19b shows the correlation between average signal intensities and measured concentrations for boron. As already shown for Mo and Si, linear agreement can neither be established for B. Concentrations of B in the range of 1 to 2 wt% exhibit the highest average signal intensities. At concentrations above 2 wt% they start to decrease again.

As already proposed with one-point calibration, it is believed that matrix effects play an important role during the ablation process. Matrix effects are caused by variable interaction of the laser pulse with the sample surface of different matrices due to variation in the properties of the investigated matrices, such as absorptivity or thermal conductivity. The mass of analyte ablated per pulse is therefore different for each matrix. Matrix effects caused by the laser ablation process lead to two related effects. First, the aerosol particles formed during the ablation process vary in particle size and geometry, which affects the transport efficiency from the ablation cell to the plasma. Second, differences in the mass load of the plasma are generated and ICP-induced matrix effects are caused, which depend on the mass of analyte ablated as well as the transport efficiency to the plasma. Vaporisation, atomisation and ionisation of the analytes introduced into the plasma are controlled by the mass load. [45]

Matrix effects caused by differences of the mass load in the plasma are amongst others responsible for the poor linear correlation between the average signal intensities and the measured concentrations. The concentrations of Mo are high compared to the ones of B and Si. This means that the major part of the formed aerosol particles consists of Mo. At concentrations below 85 wt% the energy per particle available for ionisation is high enough to ionise every Mo particle. In contrast, for samples with very high Mo concentrations more particles are generated, leading to higher mass load and the inability for ionisation of all particles. Thereby the ionisation efficiency is decreased and levels out at Mo concentrations above 95 wt%. Figure 19a suggests that at concentrations of Si below 10 wt%, which are

corresponding to concentrations of Mo above 90 wt%, the average signal intensities are suppressed due to the mass load caused by Mo. A similar assumption can be made for B, although it is difficult to make a statement for the concentrations close to 0 wt%. Higher boron concentrations lead to a high mass load in the plasma and to lower ionisation efficiencies, which is expressed in decreasing average signal intensities above 2 wt%.

As could be demonstrated, matrix effects complicate the use of conventional calibration methods such as one-point-calibration and univariate calibration for LA-ICP-MS. Therefore, it is necessary to find a calibration method which can overcome matrix effects.

4.2.3 Microscopic images of ablation craters

Interaction of the laser with the sample, particle size distribution of the generated aerosol particles and differing ionisation efficiency due to mass load in the plasma can all contribute to matrix effects in quantitative analysis using LA-ICP-MS. In this work no further investigations regarding particle size distribution and ionisation efficiency have been made, however, observations made throughout the work are based on previous works found in literature [45]. In contrast, variation in the interaction of the laser with different samples was demonstrated in this work using light microscopy.

Microscopic images of ablation craters of two samples containing very different amounts of Mo, Si and B, as created during the LA-ICP-MS measurement for one-point-calibration and univariate calibration, were compared. The laser was operated with 70 % laser power, resulting in an average fluence of 7.9 J cm^{-2}, and a repetition rate of 5 Hz (see Table 2). The material was ablated for duration of about 50s using a laser diameter of 150 µm and a scan speed of 75 µm s^{-1}.

The difference of the laser interaction with the samples, which depends on the sample composition and its properties, can be demonstrated when the ablation craters of the samples are compared. Figure 20 and 21 show cutouts of the ablation craters generated by line scans during the LA-ICP-MS analysis for sample 2 and 9.

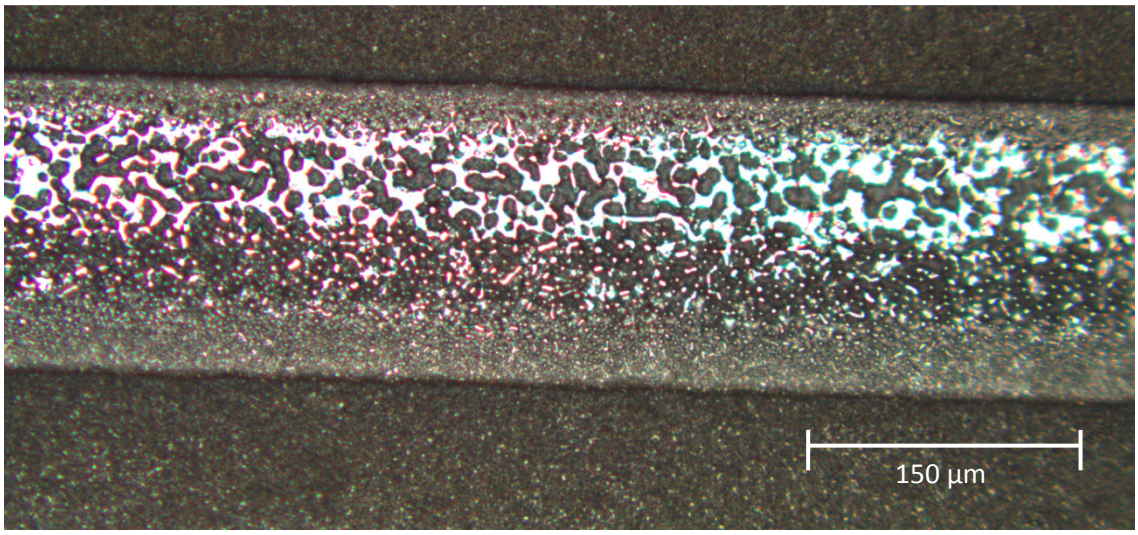

Figure 20 Cutout of a line scan of sample 2

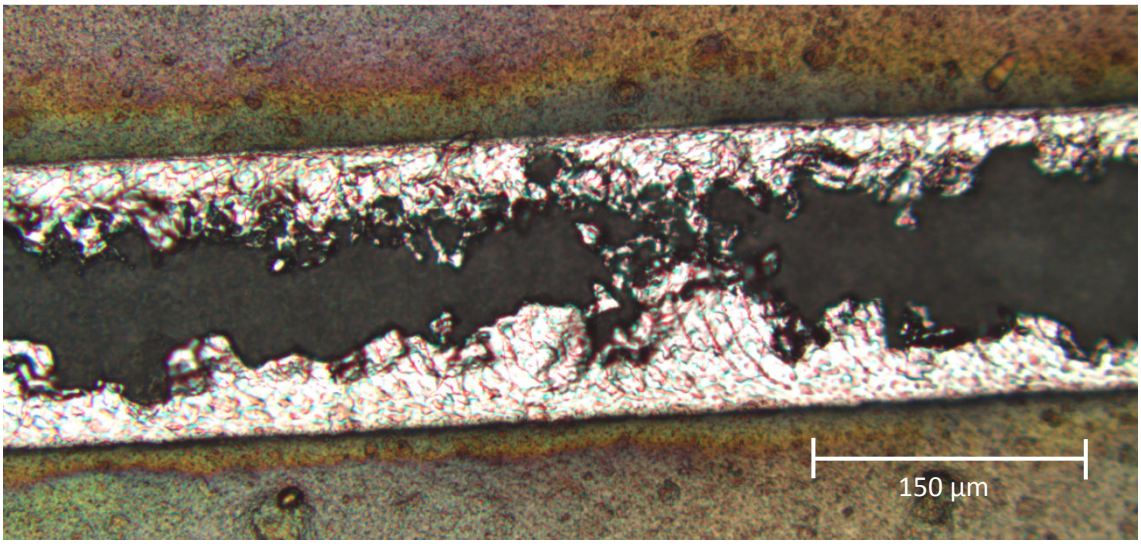

Figure 21 Cutout of a line scan of sample 9

Comparison of the images shows that the surface of the samples is different in its appearance, for example the colour. Moreover, the surface of sample 9 exhibits defects in the material, possibly inclosures.

The coating (in white colour in this image) of sample 9 is found to be fully removed at some parts of the ablation line, which can be seen on the black substrate material coming through. The amount of ablated material is particularly interesting with regard to the mass load in the plasma and the ionisation efficiency. Heat transfer into the surrounding material leads to formation of a "heat-affected zone" causing transformation of adjacent structures, which is here expressed in the form of a rainbow-coloured surface [37]. The ablation crater of sample

2 exhibits a section in the middle of the line with black and white parts of different size but approximately the same amount. The sections on the sides of the line have a different appearance and are of grey colour. In contrast to sample 9, substrate and coating material cannot be distinguished and no statement regarding the amount of the removal of the coating can be made.

The images of the line scans showed that major parts of the sample coatings are removed during the laser ablation process. In order to investigate what happens when material of the coating is removed without reaching the substrate, images of spot scans were recorded. Ablation times were adjusted in such a way that only several laser shots were used for ablation of the material. Figures 22-27 present the microscopic images of the ablation craters generated by spot scans with different ablation times for sample 2 and 9. For the spot scans the same measurement parameters, laser power of 70 %, repetition rate of 5 Hz and laser diameter of 150 µm, were used, but the ablation time was varied amounting to a number of 1, 5 and 10 shots.

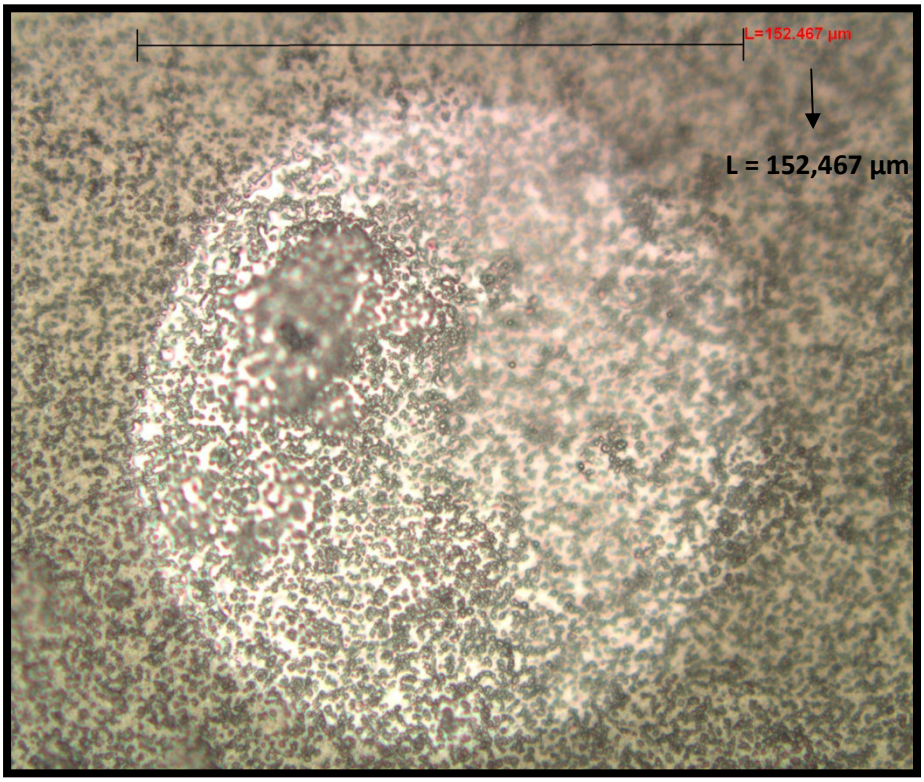

Figure 22 Ablation crater of sample number 2 after one laser shot

Figure 22 presents the ablation crater of sample 2 after a single laser shot. Sample 2 is the reference sample used for one-point calibration and exhibits the best properties considering oxidation resistance. The Mo concentration is comparably low, only exceeding 80 wt%, which results in concentrations of around 15 wt% for Si and of around 2 wt% for B. Measurement of the diameter of the crater results in only slightly larger size than the set laser diameter of 150 µm, which is due to thermal effects. This is effective for all other ablation craters in Figure 23-27. It can be seen that the sample surface, which consists of dark round parts in light-coloured background material, is generally not changed after ablation with a single laser shot. The blurred parts of the crater indicate variation in height of the sample in the range of several hundred nanometres and are probably due to redeposition of ablated material caused by melting and resolidification [37]. The microscope is only able to focus on one particular distance from the lens, resulting in a blurred view of the redeposited material, which is closer to the lens than the ablation crater. The craters generated by 5 and 10 laser shots (Figures 23 and 24) are comparable to each other and exhibit a dark background with white parts of different shape, probably representing resolidified material which was molten by the laser interaction.

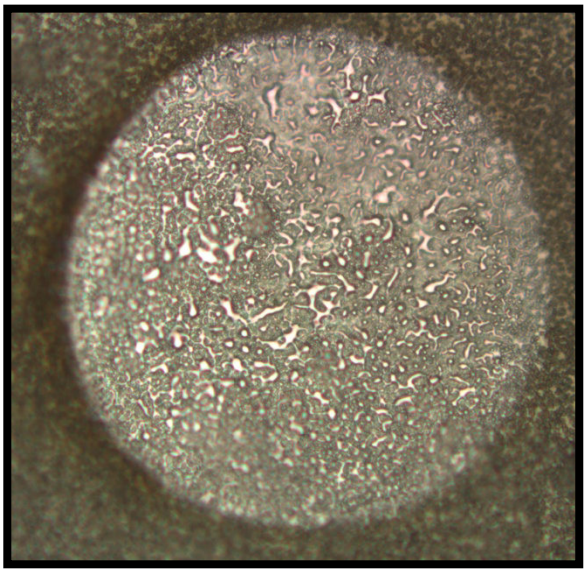

Figure 23 sample number 2, five laser shots

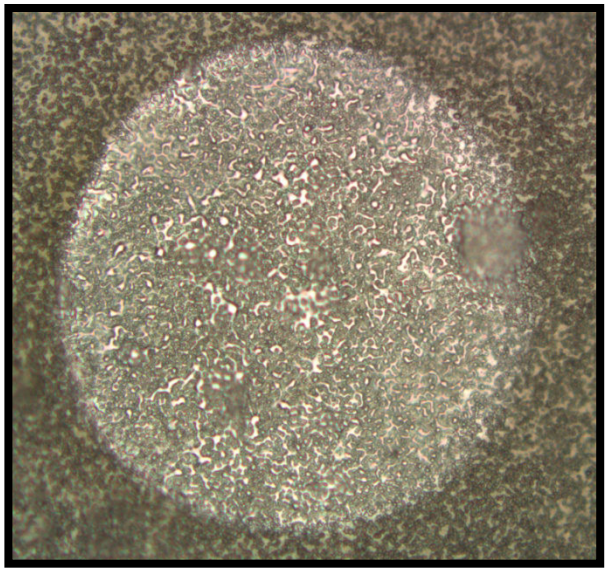

Figure 24 sample number 2, ten laser shots

In comparison, examination of the ablation craters of sample 9, which contains high amounts of Mo and less than 0,5 wt% B, leads to different effects caused by the interaction between sample surface and laser. Figures 26 and 27 show a recast layer around the rim of

the crater, as well as ejected molten material, and blurred parts which indicate redeposition of ablated material [37]. For all three craters generated by a different number of laser shots, cracks within the crater are found, which are most apparent after a single shot. They seem to develop on the surface of the material during the first interaction with the laser and are followed by generation of redeposited material. The material surrounding the ablation crater, when spot scans with 5 and 10 laser shots are used, is rainbow-coloured, as already observed for the craters of the line scans. The change of colour on the adjacent sample surface takes place at the same time as redeposition of molten material on the crater surface.

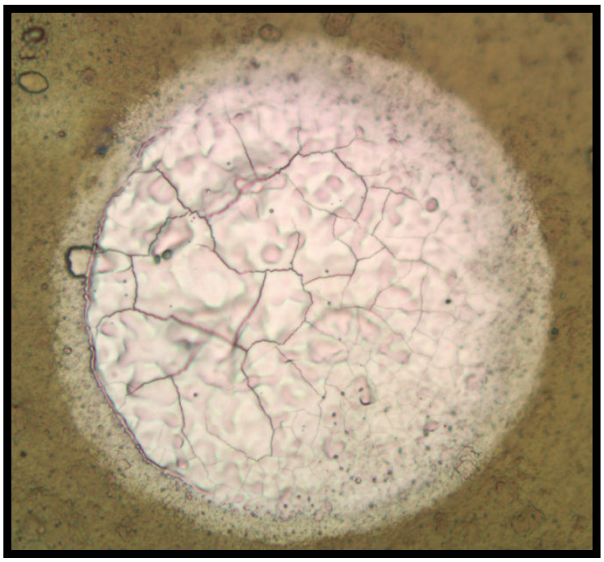

Figure 25 sample number 9, one laser shot

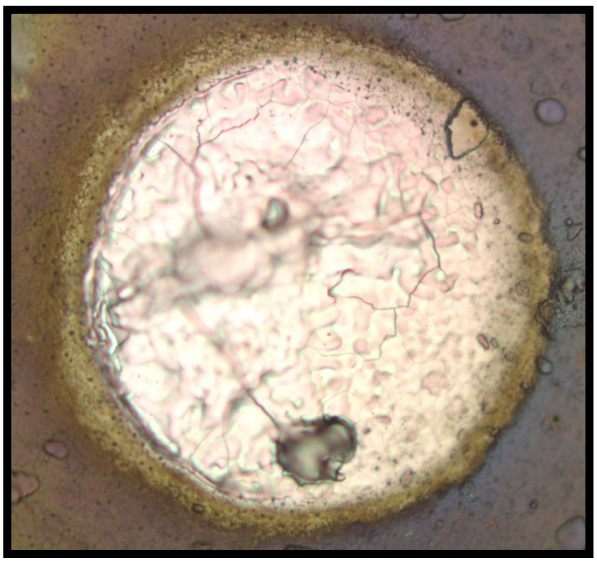

Figure 26 sample number 9, five laser shots

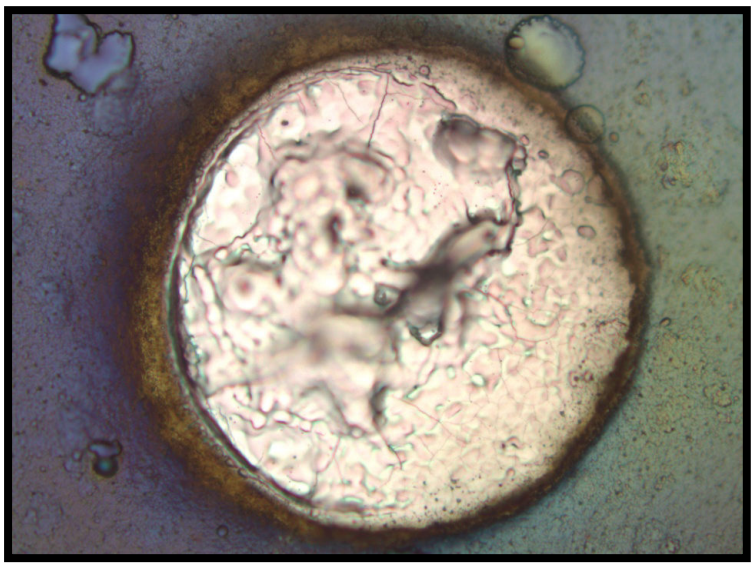

Figure 27 Ablation crater of sample number 9, ten laser shots

4.3 Multivariate calibration

In order to overcome the problem of matrix effects and quantification during the LA-ICP-MS analysis, a new approach for quantitative analysis has been investigated. Due to matrix effects the concentration of Mo, Si and B is dependent on the respective content of the analyte in the sample, as well as the concentrations of the other constituents, namely the sample matrix. Hence, a simple linear relationship between the measured signal intensities and the analyte concentration cannot be established. To describe the complex dependence of the analyte concentrations from the matrix, multivariate regression is necessary.

In literature the use of multivariate calibration to overcome limitations caused by matrix-effects was successfully applied in laser induced breakdown spectroscopy (LIBS) [46, 47]. For multivariate calibration partial least squares (PLS) regression models were used in both of the works. A multivariate calibration method used for LA-ICP-MS in various fields of analytical chemistry is principal component analysis (PCA) [24, 48, 49]. PCA is a multivariate method used for interdependent variables. It reduces the high-dimensional data with a large number of variables to a two-dimensional plane by analysing how the variables are interrelated.

Multiple linear regression (MLR) has not been reported in combination with LA-ICP-MS before, however, Chandra Mouli *et al.* [50] proposed a stepwise MLR model for solution nebulisation sampling coupled to ICP-MS.

At the beginning of the experiments with LA-ICP-MS, a survey scan with one of the samples was carried out, which means that the whole mass spectrum of the ablated material is recorded in order to determine at which m/z ratios analyte signals occur. In order to set up an MLR model, it was necessary to determine which generated ions apart from the analytes of interest have a possible influence on the measurement, as they mainly affect the plasma load and thereby the ionisation efficiency.

Figure 28 presents the results of the survey scan with the intensity (in cps) as a function of the mass (in units). Intensities for all isotopes of each element are shown, however, some masses are not determined in the survey scan due to occurring interferences. For example mass 28, which is used for determination of Si, interferes with $^{14}N^{14}N$ and mass 40 is not displayed on account of the most abundant Ar isotope. Apart from the analytes of interest,

other masses were registered that could be attributed to possible polyatomic interferences. The Na signal is assumed to be caused by impurities due to handling of the samples before the measurement.

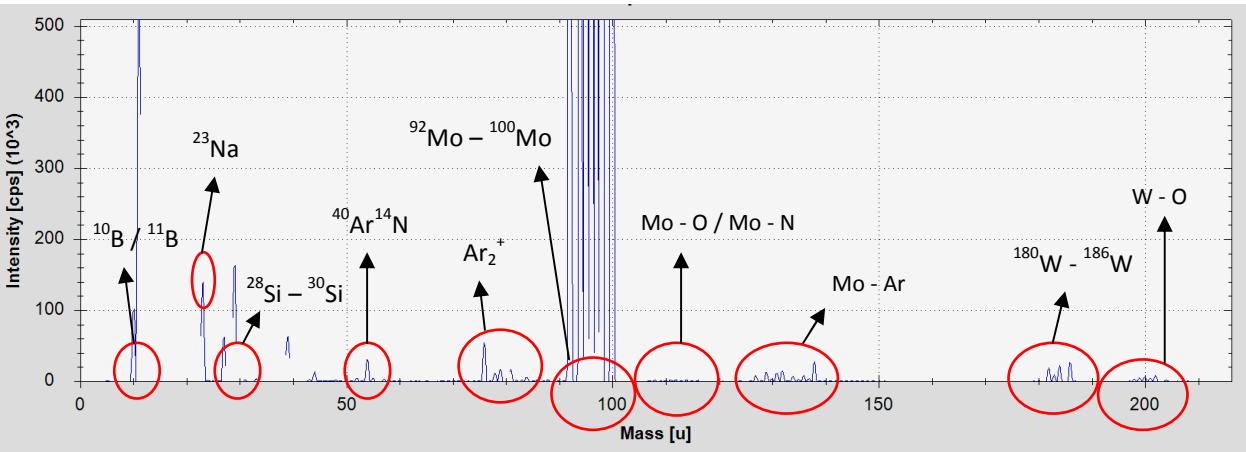

Figure 28 Survey scan of sample 7 containing analytes and possible interferences

On account of the results from the survey scan, the isotopes for further measurements were defined. Table 2 presents the measured isotopes. First of all, isotopes for the analytes of interest, Mo, Si and B, were chosen taking into account natural abundances and possible interferences (measured isotopes: ^{10}B, ^{11}B, ^{28}Si, ^{29}Si, ^{30}Si, ^{94}Mo, ^{95}Mo, ^{100}Mo). For quality control signal intensities of more than one isotope for each element were recorded. Further measured m/z ratios were ^{27}Al, ^{48}Ti, ^{184}W. Aluminum was chosen because of the substrate material and the others are probably impurities in the sample material. The rest of the measured m/z ratios are polyatomic interferences formed by reaction of the analytes with the inert gas or residual gases during the ionisation process. The polyatomic interferences represent a combination of more than one species and it is usually difficult to determine which ones contribute to the ionisation process. A selection of possible polyatomic interferences and the corresponding m/z ratios are shown in Table 5.

Table 5 Measured m/z ratios compared to the possible formed polyatomic interferences, which exhibit the same m/z ratio

Selected m/z ratios	Possible explanations for formed polyatomic interferences
44	^{40}Ar-^{4}He / ^{28}Si -^{16}O
108	^{92}Mo -^{16}O / ^{94}Mo -^{14}N / ^{28}Si-^{40}Ar-^{40}Ar
114	^{16}O-^{98}Mo
138	^{98}Mo-^{40}Ar

Background-corrected average transient signal intensities were evaluated through the LA-ICP-MS analysis by setting 5 regions with duration of 6 s within the constant transient signals. The operating parameters used during the LA-ICP-MS measurements are presented in Table 2. The signal intensities were normalised to the aluminium signal obtained in a spot scan with duration of 30 s using the same measuring parameters. The first 5-10 s of the spot scan were used to fully remove the coating. The rest of the time substrate material was ablated, providing a transient Al-signal with constant signal intensities. Analogue to the determination of background-corrected average transient signal intensities for every analyte, intensities for ^{27}Al were evaluated by setting 4 regions with duration of 4 s within the constant transient signals. Normalisation of the average signals resulted in compensation of possible instrumental drifts and better quality of the multivariate calibration model.

LA-ICP-MS signal intensities and concentrations of Mo, Si and B determined by ICP-OES analysis were used to create a multiple linear regression (MLR) model.
The model was developed at the basis of

$$y = ß_0 + ß_1x_1 + ß_2x_2 + \ldots + ß_nx_n + \varepsilon$$

where y is the measured concentration of Mo, Si or B by ICP-OES, respectively, $x_1 – x_n$ are the normalised average signal intensities of the LA-ICP-MS analysis and $ß_0$ - $ß_n$ are the regression coefficients. The model describes a regression plane in the multi-dimensional space. The parameter $ß_0$ represents the intercept of the regression plane.
Table 6 presents the number of independent variables, F-values and regression coefficients for the MLR model. The number of calibration samples is n = 10. Sample 2 and 7 are not

included in the calibration model, however, are used for external validation. For each element a multiple linear regression model was evaluated by stepwise selection of variables and corresponding regression coefficients. All specified regression coefficients differ significantly from 0. High F-values indicate good robustness of the model.

Table 6 Number of independent variables x for each element, F-values and regression coefficients given by the MLR model based on n = 10 calibration samples. m/z ratios corresponding to the regression coefficients are shown in the brackets

	Mo	**Si**	**B**
Number of variables x	5	3	4
F-value	186.9	302.5	563.2

Regression coefficients ß			
$ß_0$	554.2	2.169	-1.878
$ß_1$	-28.90 (28Si)	25.01 (28Si)	86.68 (11B)
$ß_2$	-196.4 (94Mo)	-51472 (44)	-0.499 (27Al)
$ß_3$	-296312 (108)	16920 (48Ti)	8191 (114)
$ß_4$	174449 (114)	-	692.9 (184W)
$ß_5$	-14404 (184W)	-	-

Figures 29-31 present the results of multivariate calibration. Predicted concentrations by MLR using average signal intensities obtained by LA-ICP-MS analysis are displayed as a function of the measured concentrations using sample digestion and ICP-OES.

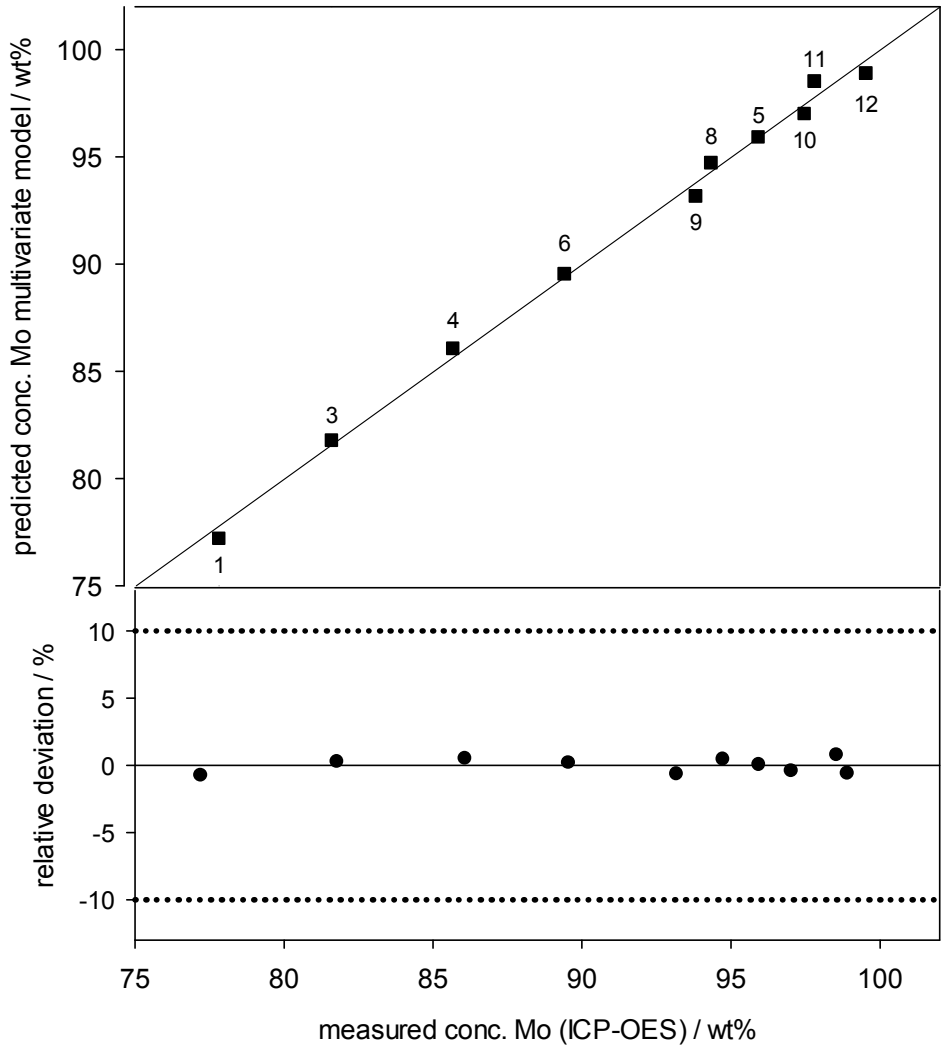

Figure 29 Concentrations (in weight %) of Mo predicted by multiple linear regression as a function of the measured concentrations (ICP-OES analysis). Relative deviations (in %) of the predicted concentrations from the measured concentrations, the dashed lines mark the 10% limit.

Figure 29 shows the correlation between measured concentrations and predicted concentrations for Mo. It is shown that excellent linear correlation can be established and that relative deviations stay below 1 %. One-point-calibration provided relative deviations for Mo within the limit, generally ranging up to 5 %, however, better relative deviations and therefore better linear agreement is achieved when MLR is used for calibration.

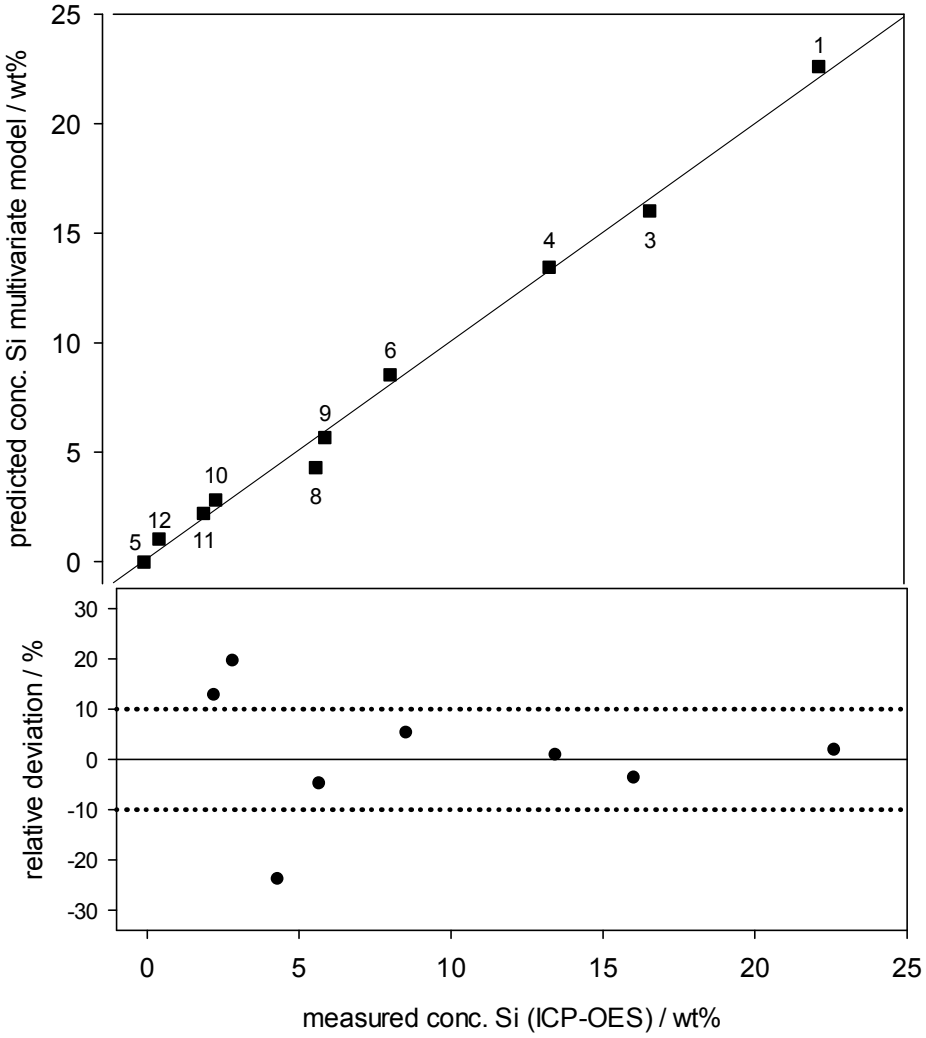

Figure 30 Concentrations (in weight %) of Si predicted by multiple linear regression as a function of the measured concentrations (ICP-OES analysis). Relative deviations (in %) of the predicted concentrations from the measured concentrations, the dashed lines mark the 10% limit.

Figure 30 presents the predicted concentrations by MLR as a function of the measured concentrations. In comparison to one-point-calibration, no trend for under-determination of Si can be observed. Good linear agreement is found when multivariate calibration is used. Sample 12 exhibits a relative deviation of around 100 % from the desired value, which is comparable to the result obtained with one-point-calibration, and is not displayed in the figure. This is due to the fact that the concentration of Si in this sample is below 0.5 wt% and therefore close to 0. Sample 5 has a concentration of 0 wt% Si and therefore no relative deviation can be specified. Only half of the samples which exceeded the limit for one-point-

calibration are outside the 10 % threshold when MLR is used. The deviation of the samples located outside the limit showed distinct improvement by decreasing from 50-100 % to only around 20 %.

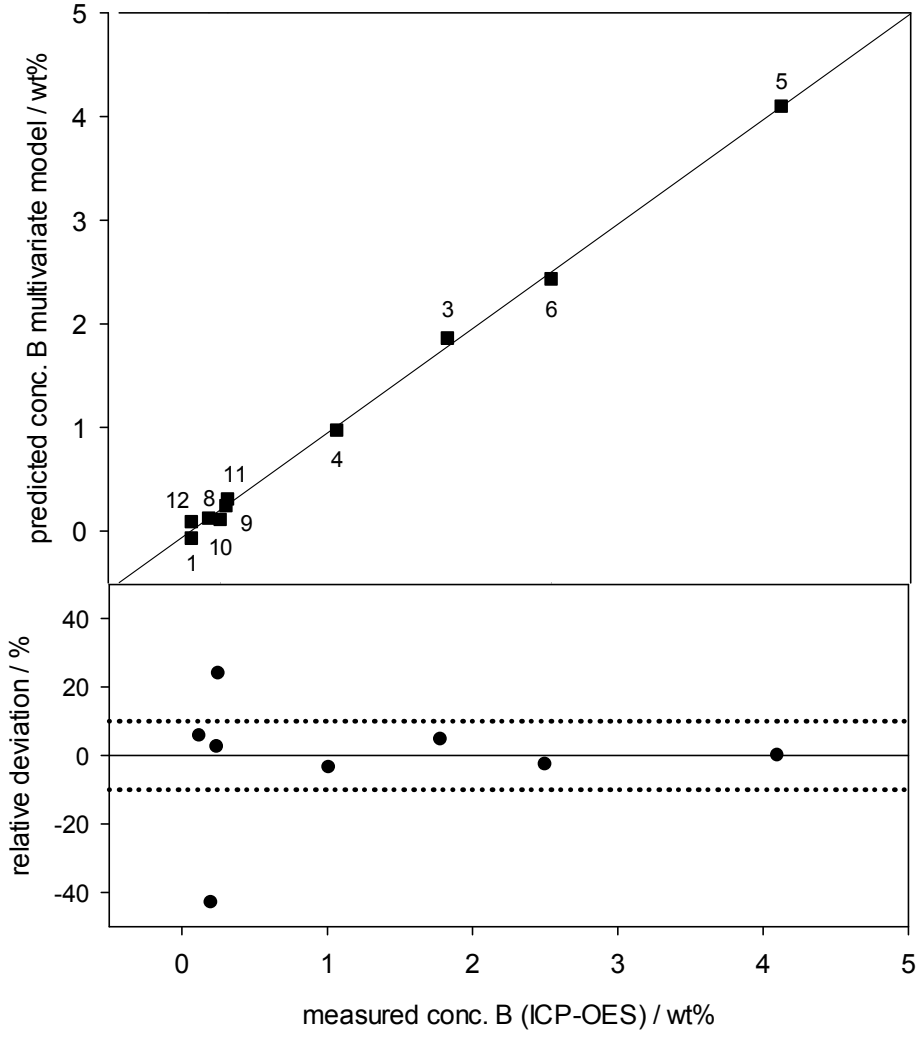

Figure 31 Concentrations (in weight %) of B predicted by multiple linear regression as a function of the measured concentrations (ICP-OES analysis). Relative deviations (in %) of the predicted concentrations from the measured concentrations, the dashed lines mark the 10% limit.

The results of multivariate calibration for B and relative deviations of the predicted concentrations from the measured concentrations are shown in Figure 31. Good linear agreement between the measured concentration by ICP-OES and predicted concentration using the average signal intensities of the LA-ICP-MS measurement can be observed. Compared to one-point calibration, where five samples had a deviation between 20 and

40%, only two samples with low concentrations exceed the 10 % limit, deviating in the same percentage range. Samples 1 and 12 have a concentration of 0 wt% B and therefore no relative deviation can be specified.

Multivariate calibration results in better linear correlation than one-point calibration for all three analytes. Concentrations of Si and B for a few samples lie outside the 10 % limit, however, the deviations are acceptable as the concentrations of the samples in question for B are close to 0. In the case of Si, these samples have concentrations below 5 wt% and only exhibit relative deviations up to 20 % which is acceptable, as it represents a huge improvement in linearity compared to one-point calibration.

In multivariate statistics the specification of degrees of freedom and calculation of the standard error is not always possible. In order to evaluate the prediction error of the calibration, the RMSEC (Root Mean Squared Error of Calibration) is specified by way of determining the PRESS value, which describes the quadratic mean of the observed residuals. It is calculated as follows, with n denoting the number of samples:

$$RMSEC = \sqrt{\frac{PRESS}{n}} = \sqrt{\frac{\Sigma\,(y_i - y_i^*)^2}{n}}$$

Low RMSEC values indicate good quality of the linear regression model. Values for Mo and Si amount to roughly 0.5 wt% and an even lower value for B is obtained (see Table 7). Coefficients of determination are above 0.99 for each analyte which demonstrates very good linear correlation.

Table 7 Coefficients of determination and RMSEC values of Mo, Si and B for multivariate calibration

Analyte	R^2	RMSEC*
Mo	0.9955	0.48
Si	0.9936	0.57
B	0.9979	0.06

* RMSEC = Root Mean Squared Error of Calibration

4.3.1 Cross-validation of the calibration model

Complicated and non-linear models usually require internal validation methods in order to test for the reliability of the model. Some linear multivariate calibration methods, such as MLR, provide theoretical foundation on the estimation of the reliability of a calibration model. Thus, additional validation is not necessarily needed, as the reliability is tested during the calculation process and can be expressed by means of theoretical values such as F-values (see Table 6).

In this work an internal validation method called cross-validation or “leave-one-out” method was applied to additionally test the reliability of the calibration model. The model data was split into two data sets, a larger one representing the “training set” and a smaller one described as “test set”. The training set was used to set up the model and the test set validated the model by applying the model to the test set. The obtained results were then compared to the expected values. In this case one of the samples was used as the test set, and the remaining nine samples formed the training set. The procedure was repeated with all ten samples, gradually defining new training and test sets in order to validate every sample of the data set.

The sum of the deviations of the results obtained by cross-validation from the expected values of a calibration model is expressed in the form of RMSECV values, which are calculated based on the same principle as the RMSEC mentioned before. Low values indicate good reliability and predictive ability of the calibration model. RMSECV values for Mo, Si and B are shown in Table 8 and are associated to the cross-validation presented in Figure 32. RMSECV values for Mo and Si are slightly higher than the RMSEC values, however, indicate good reliability of the model. For boron the two values appear to result in almost the same prediction error.

Table 8 RMSECV values obtained by leave-one-out-cross-validation

Analyte	Mo	Si	B
RMSECV*	1.57	1.04	0.10

* RMSECV = Root Mean Squared Error of Cross-Validation

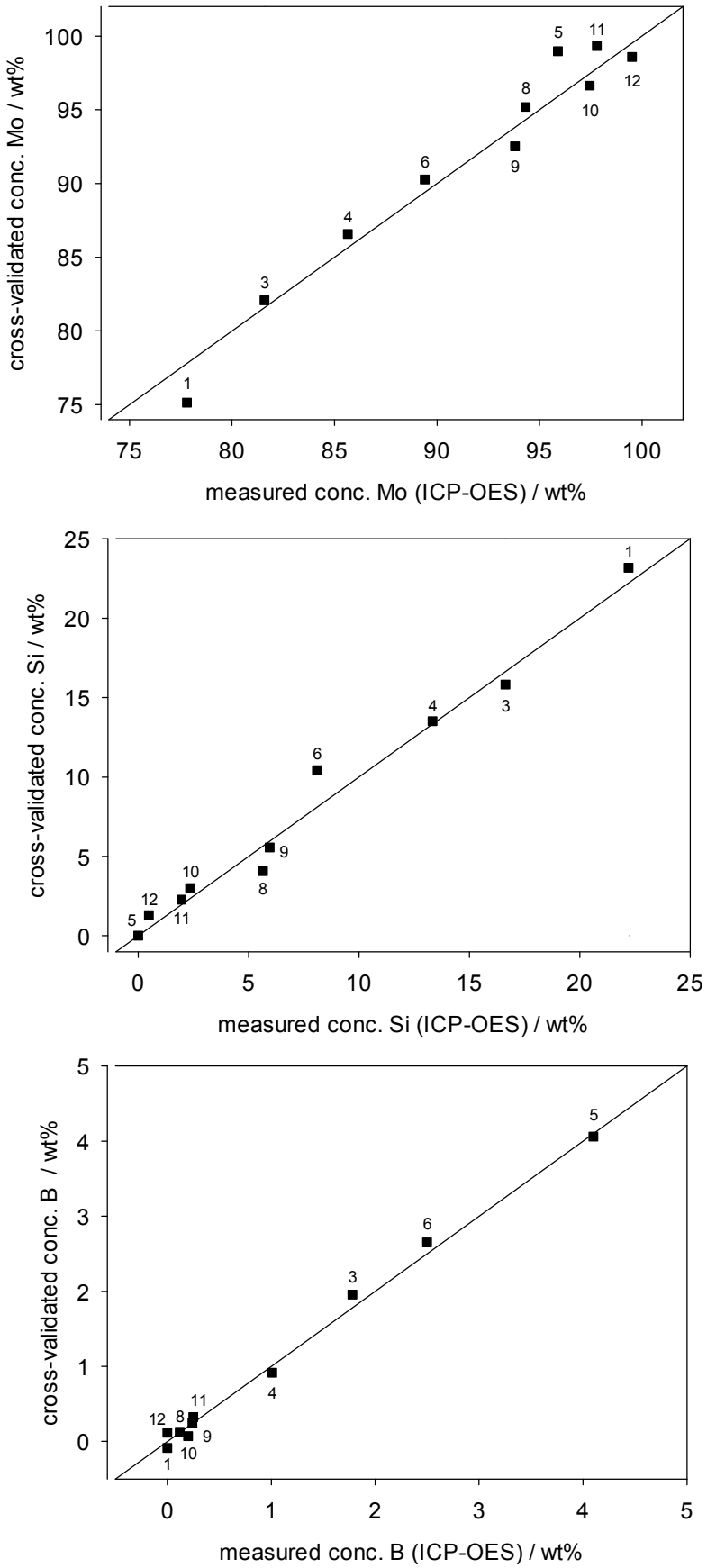

Figure 32 Concentrations of (a) Mo, (b) Si and (c) B obtained by leave-one-out-cross-validation as a function of the measured concentrations by ICP-OES

4.3.2 External validation of the calibration model

External validation is an important method for testing of the predictive ability and reliability of a multivariate calibration model. A certain number of samples within an experiment is analysed and used for the creation of a calibration model. The model is then applied to the rest of the samples and the obtained results are verified by comparison with the expected results. In this work ten samples were used for the creation of a MLR model and two samples, namely sample 2 and 7, were employed for external calibration of the MLR model.

Table 9 shows the true concentrations obtained by ICP-OES analysis compared to the predicted concentrations when the multiple linear regression model is used for prediction. Moreover, the absolute and relative deviations between true and predicted concentrations, as well as RMSEP values are presented.

Table 9 Predicted concentrations obtained by external validation of the calibration model as well as absolute deviations, relative deviations and RMSEP values compared to the true concentrations given by the ICP-OES analysis

	Analyte	Mo	Si	B
Sample 2	**True conc. / wt%**	82.77	14.99	2.24
	Predicted conc. / wt%	83.80	16.26	2.54
	Absolute deviation / wt%	1.03	1.27	0.30
	Relative deviation / %	1.24	8.48	13.18
Sample 7	**True conc. / wt%**	92.45	4.30	3.25
	Predicted conc. / wt%	93.12	4.05	3.09
	Absolute deviation / wt%	0.67	0.25	0.16
	Relative deviation / %	0.73	5.77	4.98
	RMSEP*	0.87	0.92	0.24

* RMSEP = Root Mean Squared Error of Prediction

Predicted concentrations deviate from the true concentrations around 1 wt% or below for both samples and all analytes. This results in relative deviations below or around 10 %, which is in agreement with the limits set for the calibration methods.

A small number of samples tends towards over-estimation of RMSEP values, as the number is directly included in the calculation. In this case, when only two samples are used for external validation, the RMSEP values presented in Table 9 are probably over-estimated.

RMSEP values provide comparable results to the RMSECV values obtained with cross-validation. This means that both validation methods demonstrate good reliability of the model.

5. Conclusion

In the present work a new method for the analysis of oxidation resistant coatings for ultrahigh temperature applications with different contents of Mo, Si and B was developed, which allows for fast analysis of the samples without the need of time-consuming sample preparation procedures. The properties of the coating material are strongly influenced by the Si to B ratio and only certain combinations in the Mo-Si-B system lead to outstanding oxidation resistance at high temperatures. Therefore it is necessary to know the exact composition of the coatings.

For the analysis of coatings with thickness in the micrometre range different analytical methods are used. A recently introduced method for depth profiling of thin coatings is LA-ICP-MS, which offers many advantages regarding sample design and sensitivity of the measurement. However, quantitative analysis represents a major limitation of this method due to sample related matrix effects, which result in differences between the composition of the sample and the generated aerosol particles transported to the plasma. Matrix effects are caused by variable interaction of the laser pulse with the sample surface of different matrices with differing properties, leading to changes in the mass of analyte ablated per pulse. Apart from that, size and geometry of the generated aerosol particles, which influence the transport efficiency, play an important role and can contribute to matrix effects. Interaction of the laser with the sample and particle size distribution furthermore cause ICP-induced matrix effects, which affect the ionisation efficiency inside the plasma. It was shown that problems with matrix effects also appear in this work due to the fact that the samples exhibit very different compositions of Mo, Si and B and therefore differing absorption of the laser energy. Variation in the interaction of the laser with the samples was demonstrated on two samples by comparing microscopic images of the created ablation craters.

True concentrations of Mo, Si and B for all samples were determined with high accuracy after digestion of the solid samples and following ICP-OES analysis of the obtained solutions. Sample preparation processes such as digestion are time-consuming and require the use of concentrated acids. Furthermore the risks of contamination of the sample or loss of analyte are increased.

Additionally measurements with LA-ICP-MS were carried out and three different calibration methods were tested. First, one-point calibration, being the basic approach for calibration in LA-ICP-MS, was performed with one of the samples serving as the reference sample. The concentrations determined by one-point-calibration were compared to the measured concentrations obtained by ICP-OES. It was shown that this calibration method leads to acceptable linear agreement for Mo and B, however, insufficient accuracy for quantitative analysis using LA-ICP-MS in this work. For Si no linear correlation could be observed due to a trend of under-determination of Si and relative deviations reaching 50-100 %. The samples among each other exhibit different ablation behaviour and ionisation efficiencies inside the plasma. In order to consider the influence of matrix effects, more than one standard is needed and a second calibration method, namely univariate calibration, can be applied. The precondition is linear relationship between the measured concentrations and the average signal intensities from the LA-ICP-MS analysis. It was shown that no linear agreement between the average signal intensities and the measured concentrations could be established and that univariate calibration is not suitable for quantitative analysis. As already proposed, this was attributed to matrix effects.

In order to overcome the problem of matrix effects and quantification during the LA-ICP-MS analysis, an alternative calibration method, multivariate calibration, for quantitative analysis has been investigated. A multiple linear regression model was set up, which describes the complex dependence of the analyte concentration from the matrix. It was necessary to determine which ions generated during the ionisation process have a possible influence on the analyte concentration. Therefore a survey scan was carried out and isotopes for further measurements were defined. Apart from the analytes of interest Mo, Si and B, measured m/z ratios included isotopes of ^{27}Al, ^{48}Ti and ^{184}W, as well as m/z ratios with the numbers 44, 108, 114 and 138.

The results of multiple linear regression yield to very good linear correlation for Mo, Si and B with coefficients of determination above 0.99. Relative deviations of the predicted concentrations from the measured concentrations are within the 10 % limit and deviations for Si could be decreased to values around 20 % compared to one-point-calibration. F-values

between 100 and 500 indicate good robustness of the calibration model. Cross-validation and external validation confirmed the reliability of the multivariate calibration model.

To conclude, multivariate calibration in the form of multiple linear regression (MLR) is a suitable method for accurate quantitative analysis of Mo, Si and B in oxidation resistant coatings using LA-ICP-MS in combination with ICP-OES. In future experiments a selected number of samples with known concentrations could be used for the creation of a MLR model in order to determine the unknown concentrations of additional samples, which would be analysed only using LA-ICP-MS.

6. Outlook

Up to now only a few studies covered the use of multivariate calibration for quantitative analysis to overcome matrix effects in LA-ICP-MS in literature. In particular multiple linear regression (MLR) was not reported in combination with LA-ICP-MS as a calibration method before. Therefore, the development of a multivariate model in combination with investigation of a novel material with excellent oxidation resistance in ultrahigh temperature environments represented a challenge in this work.

The major limitation of the multivariate calibration method is the small number of available samples, in particular with regard to external validation. Future work will be focused on developing a new model with a higher number of samples, which allows for external validation with more than two samples. This could lead to validation of this method as a LA-ICP-MS method without the use of matrix-matched standards. Furthermore standard samples with known concentrations could be used for setting up a multivariate model and unknown samples could be analysed without the need for a sample preparation process and subsequent ICP-OES analysis.

Further work will be directed to better understand matrix effects and their impact on the LA-ICP-MS analysis. In this context the ablation time needed to fully remove the coating will be investigated, when spot scans are carried out using two coatings with the same thickness but different composition.

Future plans from the material science point of view involve test of the reproducibility of the sputter deposition process by trying to obtain coatings of the same composition in different batches. Moreover, sputtering conditions need to be adapted in order to produce coatings of interest for ultrahigh temperature applications, which exhibit superior oxidation resistance. More focus can also be laid on investigating the effect of oxidation resistance depending on the thickness of the coatings.

Figures

Tables

Literature

1. Wasa, K., *Handbook of Sputter Deposition Technology: Fundamentals and Applications for Functional Thin Films, Nano-materials and MEMS*. 2012: William Andrew.

2. Datta, P.K., J.S. Burnell-Gray, and K. Natesan, *Coating Technology*, in *Intermetallic Compounds - Principles and Practice*. 2002, John Wiley & Sons, Ltd. p. 561-588.

3. Ohring, M., *Materials science of thin films*. 2001: Academic press.

4. Kelly, P.J. and R.D. Arnell, *Magnetron sputtering: a review of recent developments and applications.* Vacuum, 2000. **56**(3): p. 159-172.

5. Banakh, O., et al., *High-temperature oxidation resistance of Cr1−xAlxN thin films deposited by reactive magnetron sputtering.* Surface and Coatings Technology, 2003. **163–164**(0): p. 57-61.

6. Leyens, C., et al., *Recent progress in the coating protection of gamma titanium-aluminides.* JOM, 2006. **58**(1): p. 17-21.

7. Lange, A. and R. Braun, *Magnetron-sputtered oxidation protection coatings for Mo–Si–B alloys.* Corrosion Science, 2014. **84**(0): p. 74-84.

8. Heilmaier, M., et al., *Metallic materials for structural applications beyond nickel-based superalloys.* JOM, 2009. **61**(7): p. 61-67.

9. Paswan, S., R. Mitra, and S.K. Roy, *Oxidation behaviour of the Mo–Si–B and Mo–Si–B–Al alloys in the temperature range of 700–1300 °C.* Intermetallics, 2007. **15**(9): p. 1217-1227.

10. Perepezko, J.H. and R. Sakidja, *Extended Functionality of Environmentally-Resistant Mo-Si-B-Based Coatings.* JOM, 2013. **65**(2): p. 307-317.

11. Pint, B.A., J.R. DiStefano, and I.G. Wright, *Oxidation resistance: One barrier to moving beyond Ni-base superalloys.* Materials Science and Engineering: A, 2006. **415**(1–2): p. 255-263.

12. Sakidja, R., et al., *Aluminum pack cementation of Mo–Si–B alloys.* Scripta Materialia, 2006. **55**(10): p. 903-906.

13. Ritt, P., R. Sakidja, and J.H. Perepezko, *Mo–Si–B based coating for oxidation protection of SiC–C composites.* Surface and Coatings Technology, 2012. **206**(19–20): p. 4166-4172.

14. Kanický, V., H.-R. Kuhn, and D. Guenther, *Depth profile studies of ZrTiN coatings by laser ablation inductively coupled plasma mass spectrometry.* Analytical and Bioanalytical Chemistry, 2004. **380**(2): p. 218-226.

15. García, J.A., et al., *Depth profiling of industrial surface treatments by rf and dc glow discharge spectrometry.* Applied Surface Science, 2004. **235**(1–2): p. 97-102.

16. Hodoroaba, V.-D., et al., *Depth profiling of electrically non-conductive layered samples by RF-GDOES and HFM plasma SNMS.* Applied Surface Science, 2001. **179**(1–4): p. 30-37.

17. Hoffmann, V., et al., *Glow discharge mass spectrometry.* Analytical and Bioanalytical Chemistry, 2005. **381**(1): p. 173-188.

18. Pisonero, J., et al., *Quantitative depth profile analysis of boron implanted silicon by pulsed radiofrequency glow discharge time-of-flight mass spectrometry.* Solar Energy Materials and Solar Cells, 2010. **94**(8): p. 1352-1357.

19. Pisonero, J., B. Fernandez, and D. Gunther, *Critical revision of GD-MS, LA-ICP-MS and SIMS as inorganic mass spectrometric techniques for direct solid analysis.* Journal of Analytical Atomic Spectrometry, 2009. **24**(9): p. 1145-1160.

20. Pisonero, J., et al., *Capabilities of Femtosecond Laser Ablation Inductively Coupled Plasma Mass Spectrometry for Depth Profiling of Thin Metal Coatings.* Analytical Chemistry, 2007. **79**(6): p. 2325-2333.

21. Mokgalaka, N.S. and J.L. Gardea-Torresdey, *Laser Ablation Inductively Coupled Plasma Mass Spectrometry: Principles and Applications.* Applied Spectroscopy Reviews, 2006. **41**(2): p. 131-150.

22. Günther, D. and B. Hattendorf, *Solid sample analysis using laser ablation inductively coupled plasma mass spectrometry.* TrAC Trends in Analytical Chemistry, 2005. **24**(3): p. 255-265.

23. Pisonero, J. and D. Günther, *Femtosecond laser ablation inductively coupled plasma mass spectrometry: Fundamentals and capabilities for depth profiling analysis.* Mass Spectrometry Reviews, 2008. **27**(6): p. 609-623.

24. Huelin, S.R., et al., *The determination of trace elements in Fe–Mn oxide coatings on pebbles using LA-ICP-MS.* Journal of Geochemical Exploration, 2006. **91**(1–3): p. 110-124.

25. Resano, M., et al., *Laser ablation-inductively coupled plasma mass spectrometry for the fast and direct characterization of antique glazed ceramics.* Journal of Analytical Atomic Spectrometry, 2005. **20**(6): p. 508-514.

26. Deconinck, I., et al., *Capabilities of laser ablation—inductively coupled plasma mass spectrometry for (trace) element analysis of car paints for forensic purposes.* Journal of Analytical Atomic Spectrometry 2006. **21**(3): p. 279-287.

27. Trejos, T., A. Flores, and J.R. Almirall, *Micro-spectrochemical analysis of document paper and gel inks by laser ablation inductively coupled plasma mass spectrometry and laser induced breakdown spectroscopy.* Spectrochimica Acta Part B: Atomic Spectroscopy, 2010. **65**(11): p. 884-895.

28. Russo, R.E., et al., *Laser ablation in analytical chemistry—a review.* Talanta, 2002. **57**(3): p. 425-451.

29. Hou, X. and B.T. Jones, *Inductively Coupled Plasma-Optical Emission Spectrometry*, in *Encyclopedia of Analytical Chemistry*. 2006, John Wiley & Sons, Ltd.

30. WANG, T., *Inductively coupled plasma optical emission spectrometry*. 2004: Analytical Instrumentation Handbook.

31. Udupa, D.V., and Sanjiva Kumar. . *OPTICAL DESIGN OF AN ECHELLE GRATING BASED ATOMIC EMISSION SPECTROMETER FOR SIMULTANEOUS SPECTRO-CHEMICAL ANALYSIS.* 2009. csio.res.in.

32. Montaser, A., *Inductively Coupled Plasma Mass Spectrometry*. 1998: Wiley-VCH.

33. Linge, K.L. and K.E. Jarvis, *Quadrupole ICP-MS: Introduction to Instrumentation, Measurement Techniques and Analytical Capabilities.* Geostandards and Geoanalytical Research, 2009. **33**(4): p. 445-467.

34. http://rimg.geoscienceworld.org/content/53/1/243.extract.

35. Gray, A.L., *Solid sample introduction by laser ablation for inductively coupled plasma source mass spectrometry.* Analyst, 1985. **110**(5): p. 551-556.

36. Bogaerts, A., et al., *Laser ablation for analytical sampling: what can we learn from modeling?* Spectrochimica Acta Part B: Atomic Spectroscopy, 2003. **58**(11): p. 1867-1893.

37. Fernández, B., et al., *Direct analysis of solid samples by fs-LA-ICP-MS.* TrAC Trends in Analytical Chemistry, 2007. **26**(10): p. 951-966.

38. Brereton, R.G., *Introduction to multivariate calibration in analytical chemistry. Electronic Supplementary Information available. See http://www.rsc.org/suppdata/an/b0/b003805i.* Analyst 125.11, 2000: p. 2125-2154.

39. Lohninger, H., *Fundamentals of Statistics, Epina, Pressbaum*. 2012.
40. Douglas C. Montgomery, E.A.P., G. Geoffrey Vining, *Introduction to Linear Regression Analysis*. 2012: John Wiley & Sons.

41. *http://www.speciation.net/Database/Instruments/Thermo-Scientific/iCAP-6500--ICPOES-CID-Spectrometer-;i2314*.

42. *http://www.thermoscientific.com/content/tfs/en/product/icap-q-icp-ms.html*.

43. *http://www.speciation.net/Database/Instruments/New-Wave-Research-Inc/NWR213-Laser-Ablation-System-;i3105*.

44. Vieweg, A., *Thermal Stability and Oxidation Behavior of Magnetron Sputtered Mo-Si-B Thin Films*. 2014, Vienna University of Technology

45. Kroslakova, I. and D. Günther, *Elemental fractionation in laser ablation-inductively coupled plasma-mass spectrometry: evidence for mass load induced matrix effects in the ICP during ablation of a silicate glass.* Journal of Analytical Atomic Spectrometry, 2007. **22.1**: p. 51-62.

46. Laville, S., M. Sabsabi, and F.R. Doucet, *Multi-elemental analysis of solidified mineral melt samples by Laser-Induced Breakdown Spectroscopy coupled with a linear multivariate calibration.* Spectrochimica Acta Part B: Atomic Spectroscopy, 2007. **62**(12): p. 1557-1566.

47. Braga, J.W.B., et al., *Comparison of univariate and multivariate calibration for the determination of micronutrients in pellets of plant materials by laser induced breakdown spectrometry.* Spectrochimica Acta Part B: Atomic Spectroscopy, 2010. **65**(1): p. 66-74.

48. Gallo, J.M. and J.R. Almirall, *Elemental analysis of white cotton fiber evidence using solution ICP-MS and laser ablation ICP-MS (LA-ICP-MS).* Forensic Science International, 2009. **190**(1–3): p. 52-57.

49. Arroyo, L., et al., *Analysis of Soils and Sediments by Laser Ablation Inductively Coupled Plasma Mass Spectrometry (LA-ICP-MS): An Innovative Tool for Environmental Forensics.* Environmental Forensics, 2010. **11**(4): p. 315-327.

50. Chandra Mouli, P., et al., *A study on trace elemental composition of atmospheric aerosols at a semi-arid urban site using ICP-MS technique.* Atmospheric Environment, 2006. **40**(1): p. 136-146.